ABSTRACT

Title of Thesis: AN INFRARED AND LASER RANGE IMAGING SYSTEM FOR NON-INVASIVE ESTIMATION OF INTERNAL COOKING TEMPERATURE IN POULTRY FILLETS

Ling Ma, Master of Science, 2003

Thesis directed by: Associate Professor Yang Tao
Department of Biological Resources Engineering

Foodborne diseases caused by undercooked poultry products are noteworthy problems that have motivated research into the assessment of the endpoint temperature in meat. In this research, a novel infrared and laser range imaging system was proposed to estimate the internal cooking temperature of chicken breasts. It consisted of three subsystems: an IR imaging system, a laser range system, and an artificial neural network modeling system. Our experiments showed that geometric variables played an important role in the endpoint temperature estimation. The accuracy achieved by our system was 1.54° C for mean absolute error, 2% for mean absolute percent error, and 3.08(° C)^2 for mean square error. The combined IR and laser range imaging system showed

the potential for real-time, non-contact and non-invasive estimation of the internal cooking temperature in meat for enhanced food quality and safety.

AN INFRARED AND LASER RANGE IMAGING SYSTEM FOR NON-INVASIVE ESTIMATION OF INTERNAL COOKING TEMPERATURE IN POULTRY FILLETS

by

Ling Ma

Thesis submitted to the Faculty of the Graduate School of the
University of Maryland, College Park in partial fulfillment
of the requirements for the degree of
Master of Science
2003

Advisory Committee:

Associate Professor Yang Tao, Chair
Assistant Professor Y. Martin Lo
Professor Arthur T. Johnson
Professor Fredrick W. Wheaton

ACKNOWLEDGEMENT

I would like to express sincere thanks to Dr. Yang Tao, Dr. Martin Lo, Dr. Arthur Johnson, and Dr. Fredrick Wheaton for their help throughout the development of this thesis with invaluable suggestions. I also gratefully acknowledge the funding support from the USDA/NRI (United States Department of Agriculture / National Research Initiative Grant # 99-35503-8691).

Also, I wish to express my gratitude to Mr. Hansong Jing for his help in 3D image reconstruction, Mr. Gary Seibel for his technical assistance in the experimental setup and Mr. Gang Zi, Ms. Abby Vogel, Mr. Ted Andrews, and Mr. Bobak Shirmohammadi with accommodating assistance.

Finally I want to express my appreciation to all the faculty and friends at University of Maryland at College Park and my family for their support.

TABLE OF CONTENTS

LIST OF TABLES

LIST OF FIGURES

CHAPTER 1 INTRODUCTION

Food safety issues, particularly those associated with meat and poultry products, have been of serious concerns to the United States Federal Government for the last thirty years. To address these concerns, there are 21 federal agencies that work on food safety research under approximately 50 laws that directly and indirectly authorize such research (Acker, 1993). The Centers for Disease Control and Prevention (CDC) documented that there were 5,174 outbreaks of foodborne disease reported from 1988 to 1997 and these outbreaks caused 163,431 persons to become ill (Bean et al., 1997; Olsen et al., 2000).

Obviously, foodborne poisoning is noteworthy. It threatens a person's health and life. The elderly, children, and pregnant women are at heightened risk of illness or death if they eat contaminated meat or poultry products. Also, the cost of foodborne diseases is considerable. For meat and poultry products, the costs associated with medical treatment and losses in productivity caused by six of the most common bacterial pathogens are estimated at $1.8 to $4.8 billion annually (Buzby, 1996). "Preventing meat and poultry products from becoming contaminated with harmful bacteria like Salmonella or Campylobacter would

result in improved health for consumers, as well as significant economic benefits" (DeWaal, 1996).

Although the government has proposed a zero-tolerance policy for some hazardous bacteria, it is unrealistic. In fact, the "USDA argues that pathogens are ubiquitous, both on animal farms and in slaughterhouses" (Nutrition week, 1987). In addition, they gain entrance to meat and poultry products by unsanitary practices and equipment. Even random sampling programs and HACCP (Hazard Analysis and Critical Control Point (HACCP) process control systems cannot prevent foodborne hazards outbreaks. Furthermore, most outbreaks are linked to the inadequate cooking of meat and poultry products (Doyle, 1994; Veeramuthu et al., 1997; Bean et al., 1997; Olsen et al., 2000). Thus, the meat and poultry industry has changed its strategy. Instead of only reducing the bacteria multiplying in raw meat and poultry products, the industry coupled the reinforcement of hygienic handling practices with cooking meats sufficiently.

What does sufficiently mean? Clearly, if undercooked, disease-causing bacteria contained in tainted poultry will survive and threaten a consumer's health; if overcooked, the disease-causing bacteria are cooked away, as well as meat

tenderness and juiciness. To make meat and poultry products enticing for the consumer to eat, and at the same time ensuring food safety, the USDA requires minimum internal cooking temperatures for all meat and poultry products. The minimum internal cooking temperature for a chicken breast is 76.7° C (FSIS, 2001).

Currently, the concern is how to confirm that the internal cooking temperatures of meat and poultry products have reached the requirements. The purpose of this research was to solve the problem by developing an imaging system for evaluating the internal cooking temperature in chicken breasts. In addition, the system can also be used as a platform for other types of meat and poultry products. We are interested in the chicken breast, because the demand for it is high in the United States. Moreover, poultry is one of the top five single-food vehicles of outbreaks according to the report given by the Center for Science in the Public Interest (CSPI) that tracked a total of 2,472 outbreaks involving 90,355 cases from 1990 to 2002 (DeWaal and Barlow, 2002). During that period, there were 235 outbreaks with 9,612 cases linked to poultry, with chicken comprising about 37 percent of those poultry outbreaks.

Many of the problems associated with developing an imaging system result from the unpredictable thickness and shape of chicken breast specimens. This geometric variation has made it difficult to evaluate the internal cooking temperature in chicken breast. Ibarra et al. (1999) have developed an infrared (IR) imaging system to predict the internal cooking temperature in chicken breast. Furthermore, they combined an artificial neural network (ANN) with the IR imaging method to model the complicated nonlinear heat transfer process (Ibarra et al., 2000). However, the IR imaging system did not consider the chicken breasts' geometric influence and all tested samples had almost the same size and shape. In this research, a non-invasive internal cooking temperature estimation system for chicken breasts was proposed, as shown in Figure 1. Given the surface temperature and the geometric information, the ANN can instantly estimate the internal cooking temperature. It was demonstrated that 3D information played an important role in predicting the internal cooking temperature. Our contributions include:

- Instead of only relying on IR imaging, a laser range system was incorporated to extract 3D information of the chicken breast;
- A new neural network structure was defined and a better algorithm than the previous one used in Ibarra et al.'s (2000) study was used;

- The required time for the estimation of endpoint temperature was significantly shortened to twenty seconds.

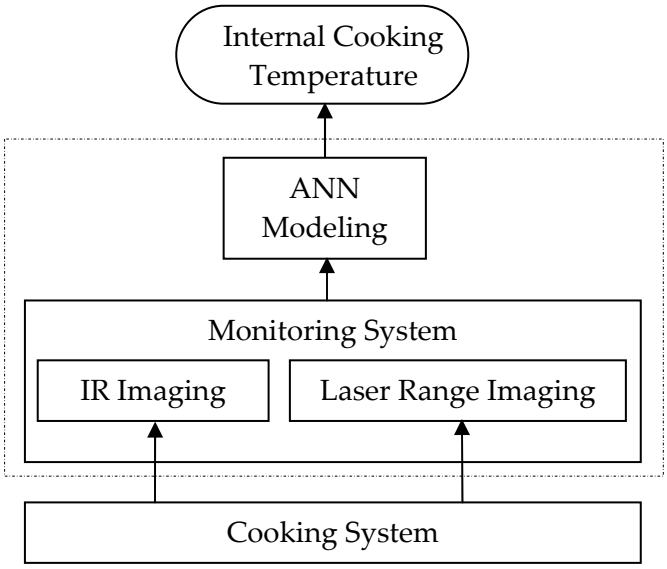

Figure 1. The structure of an internal cooking temperature estimation system.

CHAPTER 2 LITERATURE REVIEW

An imaging system was proposed for this research. The research focused on non-invasive, continuous, and real-time evaluation of the internal cooking temperature in chicken breast. To better understand this research, a brief background of foodborne diseases associated with undercooked poultry products is first introduced. Then, several approaches for measuring the internal cooking temperature in poultry meat are briefly discussed. Finally, the applications of IR imaging in food analysis and an overview of laser range imaging are presented. A brief introduction to ANN modeling is also included.

2.1 Background: Foodborne Diseases Related to Poultry Products

There are more than 40 foodborne pathogens. Four of them: Salmonella, Campylobacter, *Clostridium perfringens* (*C. perfringens*), and *Staphylococcus aureus* (*S. aureus*), are commonly harbored in poultry products (Buzby, 1996). Chicken has the greatest risk of contamination by Salmonella and Campylobacter compared to other poultry products (Doyle, 1994; DeWaal, 1996). Most outbreaks of these four bacteria in poultry are associated with the consumption of undercooked products.

Raw poultry meats are frequently tainted with pathogens. Proper handling of raw meats can reduce contamination, but cannot eradicate them. Greater than 30% of chickens processed in the United States are contaminated with Salmonella (Nutrition Week, 1987) and more than 75% of chickens and turkeys carry Campylobacter in their intestinal tracts (Beery et al., 1988).

Traditionally, cooking is done to improve the palatability of foods, but also it is the most effective way to destroy existing bacteria and minimize the chances of additional bacteria being introduced. The growth temperature and heat resistance of the four most common bacteria in poultry products are as follows:

- Salmonella

  Salmonella is the main cause of documented foodborne illnesses (CAST, 1994). It will grow at temperatures from 5 to 45° C, and the optimal growth temperature range is from 35 to 37° C (Doyle and Cliver, 1990). Storage of foods above 60° C effectively inhibits Salmonella growth (D'Aoust, 1989). Heat is one way to kill Salmonella in foods. The thermal resistance of Salmonella is mainly influenced by three factors: the strain of Salmonella, the composition of the food or the heating medium, and the water activity (Doyle and Cliver, 1990). Salmonellosis is the typical disease caused by Salmonella infections.

- Campylobacter

  Poultry is the predominant source of *Campylobacter jejuni* (*C. jejuni*), one of the Campylobacter species, which is frequently associated with campylobacteriosis in humans (Buzby et al., 1996). The growth temperature for *C. jejuni* is very narrow, from 30 to 47° C and its optimal growth temperature ranges between 42 and 45° C (Doyle, 1990). The thermal inactivation of *C. jejuni* occurs at 48° C in laboratory media (Stern and Kazmi, 1989). *C. jejuni* is highly susceptible to heat and cooking procedures adequate to kill Salmonella will also inactivate *C. jejuni* (Doyle, 1990).

- *C. perfringens*

  C. perfringens is one of the fastest multiplying bacteria. It can grow at temperatures between 15 and 50° C with an optimal growth temperature from 43 to 45° C (Labbe, 1989). The thermal inactivation of *C. perfringens* occurs at 60° C (Labbe, 1989). Furthermore, Labbe (1989) stated that *C. perfringens* is temperature tolerant, because it forms spores that can recover from temperature injury. Nevertheless, "the spores of *C. perfringens* will often germinate optimally only if they are mildly heated" (Labbe, 1989).

- *S. aureus*

Staphylococcal food poisoning is an intoxication. The temperature for the growth of *S. aureus* in foods ranges from 6.7 to 47.8° C with the optimum at 37° C. Enterotoxins are produced in the temperature range from 10 to 45° C and its optimal range is between 37 to 40° C. Above 47.8° C, staphylococci do not grow. "Heating is the most effective way to inactivate *S. aureus* in food. Heating meat to an internal temperature of 73.9-76.7° C should be sufficient to inactivate any staphylococci present" (Wong and Bergdoll, 2002).

Therefore, the endpoint temperature for chicken breasts recommended by the USDA is well above those required to inactivate the four common bacteria. According to the thermal resistance properties, poultry products should be free of bacteria if adequately cooked. Also, the rate of growth and survival of bacteria depends on pH, water activity, oxygen activity, and media nutrient level. In this study, temperature condition is the main focus.

2.2 Methods for Measuring Internal Cooking Temperature

To comply with the USDA regulations, current industrial practice is to periodically sample the endpoint temperature of meat by inserting a food thermometer immediately after cooking (Ibarra et al., 1999). This practice

measures the internal cooking temperature directly. However, it is sporadic at best, and is constrained to the exact point the thermometer is inserted, which does not ensure that all parts of the meat reached the required minimum internal cooking temperature. Additionally, the process is slow, invasive and susceptible to cross-contamination. To date, no technique has been available to inspect in real-time whether every meat product has been cooked sufficiently.

The increasing number of foodborne poisonings associated with undercooked poultry products has stimulated research to evaluate the internal cooking temperature of meat products. Several approaches have been proposed to verify that the internal cooking temperature of poultry meat has reached USDA's requirement.

Headspace gas chromatography (GC) analysis has been reported as a method to assess the adequacy of the heat treatment of chicken breasts. Ang et al. (1994) found that under the specific experimental conditions, the endpoint temperature in ground chicken breast could be expressed as a function of headspace volatile compounds using multiple correlations. To evaluate cooking history, quantitative relationships between the endpoint temperature and headspace volatiles were established at different purge temperatures of 35° C

and 50° C, respectively. At 50° C, a higher correlation was reported, because at the higher temperature, more volatiles were released from the samples. The dynamic range for that model was between 60 and 80° C. However, the headspace GC method can not be applied in food processing plants. The method is very sensitive to the sample weight, sample conditioning time and temperature, and purge time and temperature. Each variable needs to be precisely controlled, and highly trained personnel are required (Ang et al., 1994).

Many researchers have used immunoassays to determine the endpoint temperature of poultry products (Abouzied et al., 1993; Wang et al., 1993, 1994; Smith et al., 1996; Veeramuthu et al., 1997). Abouzied et al. (1993) developed a sandwich enzyme-linked immunosorbent assay (ELISA) to quantify the residual Lactate Dehydrogenase (LDH) in poultry products in order to verify the endpoint temperature. They found that additional sensitivity was obtained when a monoclonal antibody was used as a capture antibody against LDH and a polyclonal antibody was used as a detector antibody. In that assay, turkey LDH content decreased as internal cooking temperature increased. The authors indicated that turkey LDH was a better processing temperature indicator than chicken LDH.

Besides LDH, serum albumin (SA) and immunoglobulin G (IgG) were suggested by Smith et al. (1996) as additional potential indicators in turkey hams for determining the endpoint temperature. Turkey hams were processed with internal temperatures from 67 to 74° C and ELISA were developed using the three marker proteins to monitor the internal cooking temperature. With the increase of the processing temperature, the concentrations of all markers decreased. However, the authors indicated that the residual concentration of SA was too high to be a good indicator. At 68.3° C, the required internal cooking temperature for turkey hams based on USDA regulations, they reported that the residual concentration for IgG per gram of meat was 1221 ng; for LDH the concentration per gram of meat was 330 ng.

Furthermore, comparing turkey and chicken, Veeramuthu et al. (1997) investigated the influence of muscle type and temperature on the concentration of LDH, IgG, and SA. They found that the concentrations of the three endpoint temperature indicators not only varied between chicken and turkey at the same internal cooking temperature, but also differed among parts of each species. For example, chicken thigh muscle had higher concentrations of IgG than chicken breast muscle. Even for four turkey thigh products at the same endpoint temperature, the concentrations of each indicator for each product were

different. Before the ELISA became a commercial method for determining the internal cooking temperature of meats, a specific table containing the residual concentrations of protein indicators for each product was required.

However, the main disadvantage of the ELISA is that it is not sensitive enough to differentiate small temperature changes within a specific range. Wang et al. (1994) reported that the LDH ELISA did not differentiate the internal cooking temperatures of turkey thigh rolls from 68.9 to 71.1° C and the IgG ELISA did not differentiate the temperatures between 68.9 and 72.2° C.

Moreover, the above two approaches of headspace GC analysis and ELISA are complicated and time consuming. Therefore, they are not practical for on-line determination of internal cooking temperatures. Also, samples from the meat have to be extracted, making these methods invasive, labor intensive and prone to human error and variability.

Other researchers have used near infrared reflectance (NIR) and transmittance (NIT) spectroscopy to evaluate the thermal processing temperature of preheated meat products (Isaksson et al., 1989; Ellekjaer and Isaksson, 1992; Chen and Marks, 1997). Studies by Isaksson et al. (1989) suggested that NIR

was a possible method to determine the endpoint temperature of minced meat. During cooking, many physical and chemical changes occur in meat. Between 50 and 85° C, the major changes are denaturation of proteins and loss of water binding capacity. According to Ellekjaer and Isaksson's findings (1992), the absorbance in the NIR spectra (1100 to 2500 nm) was in response to the changes that occur during cooking of ground beef, scanned by a screening NIR instrument, as well as the absorbance in the NIT spectra (850 to 1050 nm). Ground beef was precooked at temperatures between 50 and 85° C at 5-degree increments. Both techniques showed equal accuracy at predicting the endpoint temperature of 'wet' beef. However, NIR predicted the temperature more accurately than NIT on freeze dried beef.

Extending the wavelength ranges to the visible spectra, Chen and Marks (1997) established a quantitative relationship to evaluate the cooking history of chicken breast meat patties by reflectance spectroscopy. This method predicted the cooking time and internal cooking temperature. Multilinear regression techniques were used to develop calibration equations. Comparing three wavelength ranges: visible (400 to 700 nm), near-infrared (1100 to 2500 nm), and visible/near-infrared (400 to 2500 nm), the authors concluded that reflectance gave better calibrations for prediction of thermal history than transmittance

regardless of which spectra. And for reflectance spectroscopy, visible/near-infrared spectra resulted in the best evaluations.

Reflectance spectroscopy makes it possible to rapidly and nondestructively measure the internal cooking temperature of poultry meat. However, drawbacks still exist. Well-trained operators are needed to handle the process properly and extensive calibration standards are used. Moreover, the method is limited to absolutely regular shapes of meat products. All sample patties used in the experiments must have the same thickness and diameter.

It is well known that the intensity of IR images is closely related to the sample's surface temperature. This characteristic makes IR imaging a promising technique for quickly and non-invasively inspecting endpoint temperatures in meat products. Ibarra et al. (1999) developed a method using IR imaging to estimate the internal cooking temperature in chicken breasts. An autoregressive time series model was proposed to correlate the surface temperature with the internal temperature in each chicken breast after cooking. In that study, an IR camera was used to capture the IR images of the chicken breast. For calibrations, the internal temperatures of the chicken breasts were recorded by thermocouples (TCs). Time series observations of simultaneous internal and

external temperatures were obtained for 570 seconds at 30-second intervals immediately after the cooking process. Figure 2 illustrates the experimental setup and shows the IR images of the cooked chicken samples. The autocorrelation and the partial autocorrelation of external temperatures and the cross-correlation between the internal and external temperatures were calculated. The statistical analysis of experimental data indicated that the internal temperature could be estimated by using three surface temperature lags at times 0, 60, and 150 seconds after cooking. Therefore, this linear modeling required three IR images and 150 seconds for estimation of internal cooking temperature.

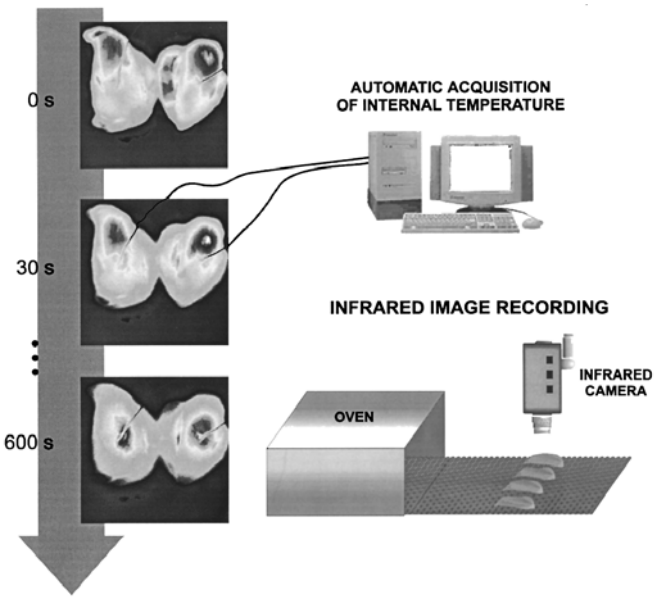

Figure 2. Experimental configuration and thermal images of samples (Ibarra et al., 1999).

Furthermore, taking into account the nonlinear property of the heat transfer process, Ibarra et al. (2000) combined IR imaging with ANN modeling to enhance the time series analysis. In that work, a five-layer feed forward ANN was proposed and the Levenberg-Marquardt (LM) algorithm was used because of its high speed and convergence. The ANN input was a vector composed of external temperature lags; the output was the predicted internal temperature.

Assuming that only six lags significantly contribute to the estimation, the number of external temperature lags input into the ANN was reduced dramatically. And by analyzing the covariance matrix of internal and external temperatures within six lags, the number of external temperature lags was further reduced to two. To test if two lags were enough for the endpoint temperature estimation, two cases were presented. One was case [01] in which the inputs were only composed of simultaneous and one-lag (30 seconds after cooking) external temperatures; the other was case [012] in which an additional second lag (60 seconds after cooking) external temperature was added to the inputs. Case [01] with fewer temperature lags resulted in better performance for estimation of internal cooking temperature than case [012]. The ANN method shortened the required estimation time to 30 seconds and only required two IR images.

Thus, IR imaging is a potential alternative approach for the real-time assessment of the internal cooking temperature in chicken breasts. It ensures all chicken meats be inspected thoroughly, quickly, and non-invasively, thereby eliminating the possibility of cross-contamination. The chicken samples used in Ibarra et al.'s experiments (1999 and 2000), however, had similar shape and thickness, which is not the usual case. Variable shapes and thicknesses may directly affect the heat transfer process in meats. Therefore, in this research, a laser range system was incorporated with an IR imaging system to extract the 3D information of the chicken breast.

2.3 Infrared (IR) Imaging in Food Analysis

IR imaging is an emerging technique in the field of food analysis. The theoretical foundation behind this technology is described by the Stefan-Boltzmann law as follows:

$$E = \sigma \varepsilon T^4 \quad (1)$$

where E is the radiation intensity of an emitter; σ is the Stefan-Boltzmann constant (= 5.7 X 10^{-8} W/m^2K^4); ε is emissivity, a material property of the object, which is often available in the literature; and T is the absolute surface temperature of the object. The intensity emitted depends on the fourth power of the surface temperature of the object.

The non-contact characteristic of IR imaging is an obvious advantage. IR imaging surpasses conventional thermal sensors for the following conditions:

- To measure the surface temperature of solid or liquid materials for which it is difficult to utilize a probe;
- To measure the temperature of some material that can erode the probe or reduce its usage time;
- To monitor the temperature of materials inside a closed chamber such as a microwave oven.

Also, the nondestructive, high-speed, automatic monitoring and accuracy make IR imaging the preferred method in many cases.

Goedeken et al. (1991) introduced a method to continuously monitor the surface temperature of food in a microwave oven. Traditional temperature sensors could not be applied in microwave heating. Instead, the authors used an IR imaging system to determine the surface temperature distribution in food heating in the microwave oven. The top section of the microwave cavity was removed and replaced with a hardware cloth screen so that the IR camera could see through the screen onto the sample during heating. However, the screen interfered with the IR measurement. A multivariable regression model was used to calibrate the system. To obtain the dielectric constant of a sample,

Cuccurullo et al. (2002) proposed a technique using IR thermography to measure the surface temperature of the sample in microwave heating. To simplify the analytical model, the sample was confined to a cylindrical box and the preliminary experiments were tested using water samples.

Fang and Shah (1998) carried out an IR imaging investigation on the heat transfer through air/water and oil/water interfaces. Their aim was to investigate the effect of surfactant monolayers on the heat transfer process through the interfaces. To do this, an IR camera was used to monitor the surface temperature of water and oil. The time required for the surface temperature to increase by 1° C was recorded as a criterion to show the effect of surfactant monolayers on heat transfer. The experimental data revealed that with a monolayer at the air/water interface, the time required for the temperature to increase was shorter than without a monolayer, in that the monolayer reduced the effect of evaporative cooling. Also, at the oil/water interface, the presence of a monolayer increased the heat transfer resistance. Thus, longer time was required to increase the surface temperature.

The IR imaging technique was also used to assess the ripeness of fruits. In an early work, Danno et al. (1980) used an IR vidicon camera to measure the

surface temperature in fruits for evaluation of the grade of maturity. Usually, changes in metabolism due to the stage of ripeness caused small surface temperature differences. By adjusting the storage temperature, the small temperature differences could be detected using an IR camera. Japanese persimmon, Japanese pear and tomato were selected for the tests under different storage conditions. It was reported that when stored at a lower temperature (5° C), the surface temperature of the mature and overripe fruits was lower than those of the immature ones; reversely, when stored at a higher temperature (30° C), the surface temperature of the mature and overripe fruits was higher than those of the immature ones. Using the aid of thermal imaging analysis, Hellebrand et al. (2001) explained that the transpiration process was related to the surface temperature change of fruits. Mostly, the maximum value of transpiration resistance coincided with the stage of ripeness.

Intensive research has been done on detecting defects of fruits using an IR imaging technique. Tao (1996) developed an IR imaging system for on-line apple defect inspection. The difference in thermal diffusivity between bruised and sound tissues caused divergent surface temperatures (Varith et al., 2000). Varith et al. used a ThermaCam™ PM390 and indicated that bruises could be detected only during the cooling or heating process. After that, the surface

temperature of bruised or sound tissues reached thermal equilibrium. In general, within 30 to 180 seconds after heating, the bruises of apples were up to 1-2° C lower than the sound tissues. They found that it was easier to detect the bruises using a heating treatment than a cooling treatment. Varith et al. (2001) advanced their study by using a finite element model to validate the bruise detection by thermal imaging. Their findings determined that: 1) the surface temperatures of bruises increased and decreased slower than those of sound tissues; 2) the divergent surface temperatures between bruised and sound tissues were not only associated with the difference in thermal diffusivity, but were also related to an effective convective heat transfer coefficient and time; and 3) bruises had a higher thermal diffusivity value than sound tissues; Nevertheless, the one problem that still existed for on-line apple defect sorting was how to distinguish between true defects and stem-ends/calyxes in IR images. To solve that problem, Wen and Tao (2000) presented a combined near-IR (NIR) and mid-IR (MIR) imaging method. True defects and stem-ends/calyxes could be detected using a NI camera, while using a MIR camera, only stem-ends/calyxes could be detected. Therefore, by subtracting the MIR image from the corresponding NI image, only the true defects remained.

2.4 Laser Range Imaging

Laser range imaging is a well-established technique for 3D image reconstruction. It is based on the triangulation relationship between two lines (DePiero and Trivedi, 1996): one along the laser optical axis and the other along the camera sighting direction (see Figure 3).

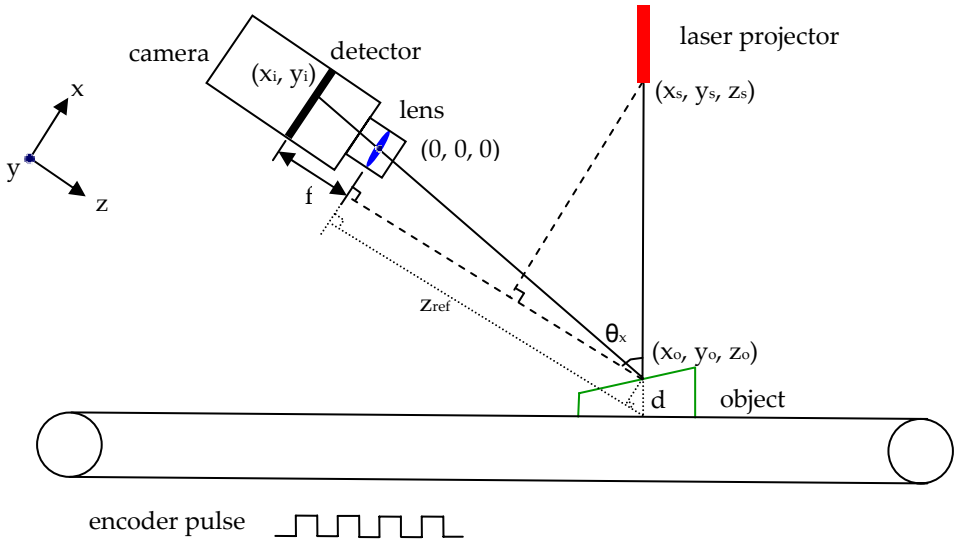

Figure 3. Geometrical model of the triangulation (y is pointing out from the paper).

General equations describing the triangulation were derived by Jalkio et al. in 1985. As shown in Figure 3, the origin of coordinates is the imaging lens center. A single laser light emitted from the laser projector is represented at angles θ_x and θ_y to the z-axis in the x and y directions, respectively. The object is illuminated at the point (x_o, y_o, z_o):

$$x_o = x_s - (z_o - z_s)\tan\theta_x$$
$$y_o = y_s - (z_o - z_s)\tan\theta_y \quad (2)$$

where (x_s, y_s, z_s) are the coordinates of the light source. The camera detects this point and forms an image on its detector plane at (x_i, y_i):

$$x_i = \frac{f}{z_o}x_o = \frac{f}{z_o}(x_s + z_s\tan\theta_x) - f\tan\theta_x$$
$$y_i = \frac{f}{z_o}y_o = \frac{f}{z_o}(y_s + z_s\tan\theta_y) - f\tan\theta_y \quad (3)$$

where f is the distance between the camera's imaging lens and its detector plane, which is nearly equal to the focal length of the camera for long working distances. Compared to an image point formed by an object a known distance away, the displacements between the two points are Δx_i and Δy_i:

$$\Delta x_i = f(x_s + z_s\tan\theta_x)\left(\frac{1}{z_o} - \frac{1}{z_{ref}}\right)$$
$$\Delta y_i = f(y_s + z_s\tan\theta_y)\left(\frac{1}{z_o} - \frac{1}{z_{ref}}\right) \quad (4)$$

where z_{ref}, the distance of the reference object, is known. Any one of the displacements can be used to calculate the object distance. If the x displacement is chosen for calculation, the distance z_o is given by

$$z_o = \frac{z_{ref}}{1 + \Delta x_i z_{ref}/f(x_s + z_s\tan\theta_x)} \quad (5)$$

If the displacements are restricted only in the x direction, which means $\Delta y_i = 0$, then $y_s = z_s = 0$. Furthermore, equation 5 can be simplified to

$$z_o = \frac{z_{ref}}{1 + \Delta x_i z_{ref} / f x_s} \tag{6}$$

In Figure 3, if the surface of the conveyor platform is chosen as the reference, the depth of the object can be calculated by

$$d = \frac{(z_{ref} - z_o)}{\cos \theta_x} \tag{7}$$

Therefore, once the relative position of the camera and the laser projector are known, the distance to the object and the thickness information can be calculated. When the object moves (e.g. with the conveyor) under the laser range system, the distance of each point on the object is obtained and then the 3D information of the object is extracted.

The laser line screen scans the object. The conveyor belt and the camera are synchronized by an encoder pulse (see Figure 3). The length direction resolution r_L for the 3D image of the object is equal to the pulse width. The height direction resolution r_h can be determined by the image pixel resolution. In other words, with a 200 x 640 image size, r_h = image field length (mm) / 200

pixels. The width direction resolution r_w, similar to the height direction resolution, can be determined by r_w = image field width (mm) / 640 pixels.

2.5 Introduction to Artificial Neural Network (ANN)

There are many modeling methods. In general, one way is to develop a model which uses physically meaningful equations or empirical equations to represent the system; an alternative is as ANN, which is a system of equations that do not have a physical meaning. Each model has its own drawbacks and advantages. The first one, mathematically, expresses the physical process, which is its strength, but also its weakness. For complex systems, such as heat transfer, the cooking process which involves many physical and chemical changes is difficult to simulate with a few meaningful equations.

The ANN is composed of nodes. The highly interconnected nodes make the ANN capable of adjusting to a specific problem. Also, the ANN can model a system without a priori knowledge of the process variable relationships (Ramesh et al., 1996). However, without favorable training samples, the ANN could result in poor generalizations.

Several types of ANNs exist. The Multi-layer perceptron (MLP) network is one of the most commonly used neural network architectures. Its structure is shown in Figure 4. Nodes in the ANN are loosely based on biological neurons and they are highly interconnected. Nodes in the input layer respond to inputs by (Hagan et al., 1995)

$$\begin{aligned} a^0 &= p \\ a^1 &= f^1\left(W^1 a^0 + b^1\right) \end{aligned} \tag{8}$$

where a^1, f^1, W^1, and b^1 are the outputs, transfer function, weights and biases of the input layer, respectively; and $a^0 = p$ are the inputs. Then the signal is transferred forward to nodes in the hidden layers in a similar way. Finally, outputs are produced from the output layer by (Hagan et al., 1995)

$$\begin{aligned} a^M &= f^M\left(W^M a^{M-1} + b^M\right) \\ a &= a^M \end{aligned} \tag{9}$$

where $a = a^M$ are the outputs; f^M, W^M, and b^M are the transfer function, weights and biases of the output layer, respectively; and a^{M-1} are the inputs of the output layer which are the outputs of the (M-1) layer.

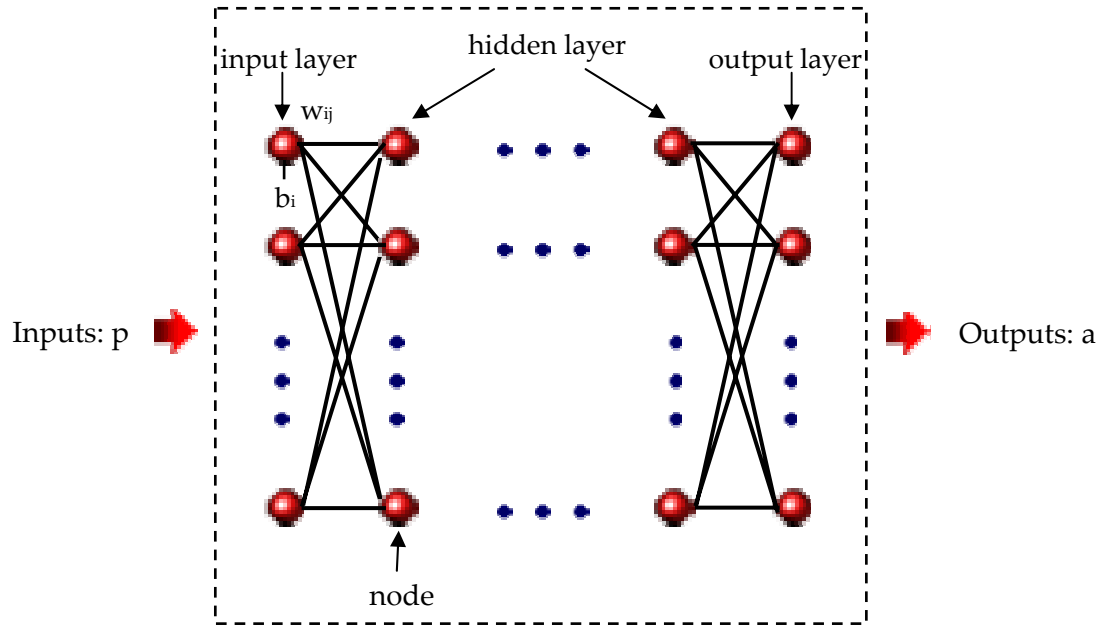

Figure 4. Topology of MLP network.

The values of weights and biases are obtained by a training (or learning) process using training samples (or training data). For supervised training, the training samples come from experiments or an experimentally validated model. They are the combination of inputs and true outputs. During the training process, a true output is called a 'target'. The weights and biases are adapted by a learning algorithm (or learning rule), which try to optimize the 'performance' of the network. The 'performance' of the network is defined by a performance index, such as mean square errors (MSE) or sum of square errors (SSE), which can be quantitatively calculated. The smaller the performance index is, the better the network performs. Following the training process, the correlation between inputs and outputs is obtained and the adapted weights and biases

will not change until the ANN is relearned with new training data. Then the testing process is implemented to ensure that the trained ANN is not overfit or underlearned and still performs well enough with new data.

Learning is an iterative process. It gradually improves the network performance by decreasing the performance index value. The performance goal is defined as a threshold value. When the performance index is less than performance goal, the learning process terminates. The basic procedure for the learning process is shown in Figure 5. The first step in the training is to initialize weights and biases. With the initial weights and biases, the outputs are calculated by inputting all training data into the ANN. The third step is to calculate the performance index. Then the performance index is compared to a given performance goal. If it is larger than the performance goal, weights and biases are adjusted. Subsequently, the outputs and the performance index are recalculated using the updated weights and biases. The process is repeated until the performance index is less than the performance goal. Numerous learning algorithms exist. The key difference among them is how each adjusts the weights and biases to reach the predetermined performance goal.

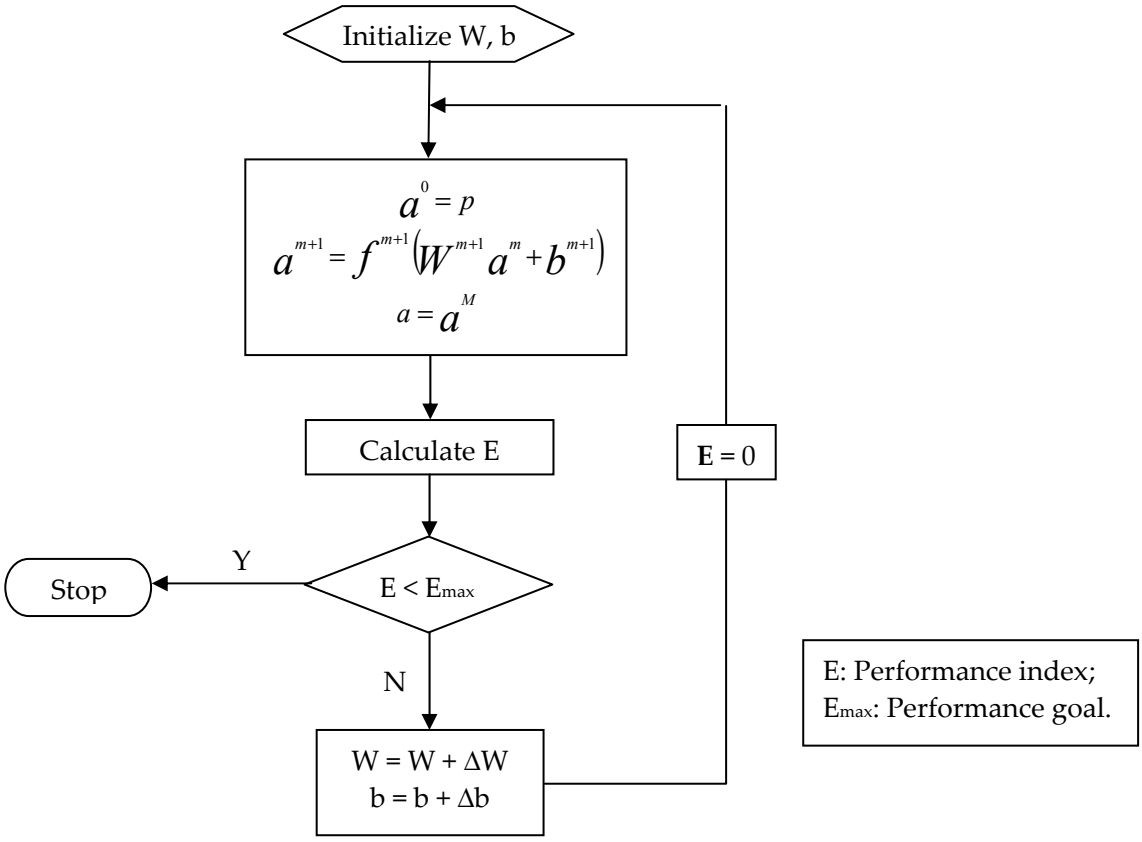

Figure 5. Flow chart for learning process.

Recently, ANNs have been widely used in food processing related problems. Mittal and Zhang (2000a, b, c, and 2001) used an ANN method to predict the 1) freezing time for food products with any shape; 2) temperature and moisture content of frankfurters during smoke-house cooking; and 3) temperature, moisture, and fat contents in slab-shaped foods and meatballs with edible coatings during deep-fat frying. Lou and Nakai (2001) used an ANN to compare with a response surface methodology to estimate the maximum specific growth rate and lag phase of Lactobacillus sake in modified-

atmosphere-packed cooked meat products. Hussain et al. (2002) combined an ANN with a regression polynomial-based model to predict pore formation in foods during drying.

CHAPTER 3 OBJECTIVES

The overall objective of this study was to develop a novel non-invasive endpoint temperature estimation system for chicken breasts. The developed system was composed of three subsystems: an IR imaging system, a laser range system, and an ANN modeling system. The IR imaging system was used to obtain the surface temperature of chicken samples. The laser range system was used to get the 3D information about the samples. The ANN system was used for modeling the nonlinear heat transfer process. Given the surface temperature and the 3D information, the trained ANN could instantly estimate the internal cooking temperature.

The specific objectives were to:

1. Establish the mapping relationship between the inputs, including surface temperature and geometric information, and the output which was the internal cooking temperature of meat; and
2. Examine the effects of external temperature lags and geometric information on the estimation performance.

CHAPTER 4 EQUIPMENT

The imaging system developed in this research consisted of three major parts: 1) an IR imaging station; 2) a laser range system; and 3) internal temperature recording.

4.1 IR Imaging Station

The IR imaging station consisted of an oven, an IR camera, and a host personal computer (PC) platform. Chicken breasts were cooked inside the oven. Following cooking, they were removed from the oven by the conveyor belt, and passed through the field of view of the IR camera. A sequence of IR images was grabbed and stored in PC memory.

4.1.1 Oven

An Impinger Conveyor Oven (Model series 1100), produced by Lincoln Foodservice Products Inc., was used in the experiment to simulate industrial cooking conditions (see Figure 6). A specially designed fan inside the oven converts the energy from a heat source (electric) into a high velocity air stream. The heating process inside the oven is called "Air Impingement"; where air acts

as the medium to heat the food products. The oven is equipped with an adjustable speed conveyor belt. The length of the belt can be extended and the belt's transferring direction can be reversed. The cooking temperature inside the oven can be set from 121.1 to 301.7° C (250 to 575° F) and is adjustable in five degree increments (F mode). The cooking time, which depends on the belt speed, has a range from 1 to 30 minutes. As well as cooking temperature, cooking time is displayed in real-time.

4.1.2 IR Camera

A Merlin uncooled thermal camera (Model No. 414-0060-10, Indigo Systems Corporation) shown in Figure 7 is the key component of the system. The spectrum range of the camera is from 7 to 14 microns. In this waveband, IR transmission is minimally affected by the interference of steam and smoke during the cooking and cooling processes. The camera has a Focal Plane Array (FPA) incorporating a matrix of microbolometer detectors with a measurement range from 0 to 500° C. It was mounted above the conveyor platform of the oven with an adjustable height frame. The camera features are operable by a remote button panel. A Citizen LCD monitor (Model No. M938-1A, Japan CBM Corporation) was used to adjust the camera focus. In addition, the captured thermograms were transported by a RGB cable to a host Pentium® IV PC

platform equipped with a Matrox Meteor II image board. Software Matrox Inspector 2.2 (Matrox Electronics Systems Ltd., Quebec, Canada) was installed to program the grabbing and analysis processes of the IR images. The PC's operation system was Windows 2000.

Figure 6. The Lincoln Impinger Oven.

Figure 7. The Merlin IR camera.

4.2 Laser Range System

A laser range system, shown in Figure 8, was implemented to determine the irregular 3D information of the chicken breast. It contained a red laser line projector and a monochromatic CCD camera (TM-6703) from Pulnix Company. The red diode laser was used because of its low price and simplicity. Additionally, to reduce the noise and avoid ambient light interference, a 650nm long-pass filter (LL-650-F) produced by Corion Inc. was incorporated with the camera. The camera and the laser line projector were mounted on the same stationary frame. The camera was connected to a Matrox Genesis LC board hosted in the PC. An electronic encoder was implemented to synchronize the conveyor belt with the CCD camera. The 3D images of chicken breasts were reconstructed and saved in the PC. 3D images were processed with 8 bits resolution using software Matlab 6.1 (The Mathworks Inc., MA, USA). Also, the laser light did not interfere with the mid-infrared imaging.

4.3 Internal Temperature Recording

The actual internal temperatures of the breasts were recorded by twelve thermocouples (TCs) during the cooking and cooling processes. A type-T thermocouple (TC) was chosen, because its measurement range from -270 to 400° C matches the food operating temperature. More importantly, the type-T

TC is resistant to moisture which usually occurs during food processing. The TCs used in the experiment were purchased from Omega Company with 150 mm probe length and 0.50 mm probe diameter, as shown in Figure 9. The length and diameter of the probe made it easy to insert into the chicken breast and it also dispersed the surface heat quickly. Before cooking, the thickness of each chicken sample was measured by a Dial Height Gauge shown in Figure 10 to mark the thickest part. Then, a TC was inserted into the center of the thickest part. A 16-channel thermocouple/voltage input Omega data acquisition board, as shown in Figure 11, automatically recorded the temperatures into the PC using DASwizard software (Measurement Computing Corporation, MA, USA). The board has screw terminals for each TC channel and a cold junction sensor integrated into an isothermal bar. After cooking, the internal temperatures of the chicken breasts measured by the embedded TCs were treated as the "ground truth" values to compare with the predicted internal temperatures.

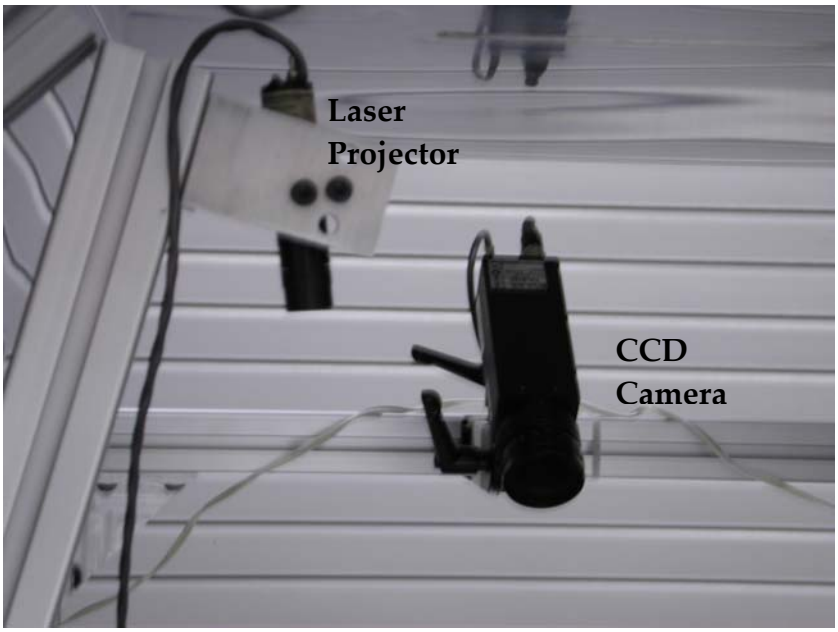

Figure 8. The laser range system for 3D image reconstruction.

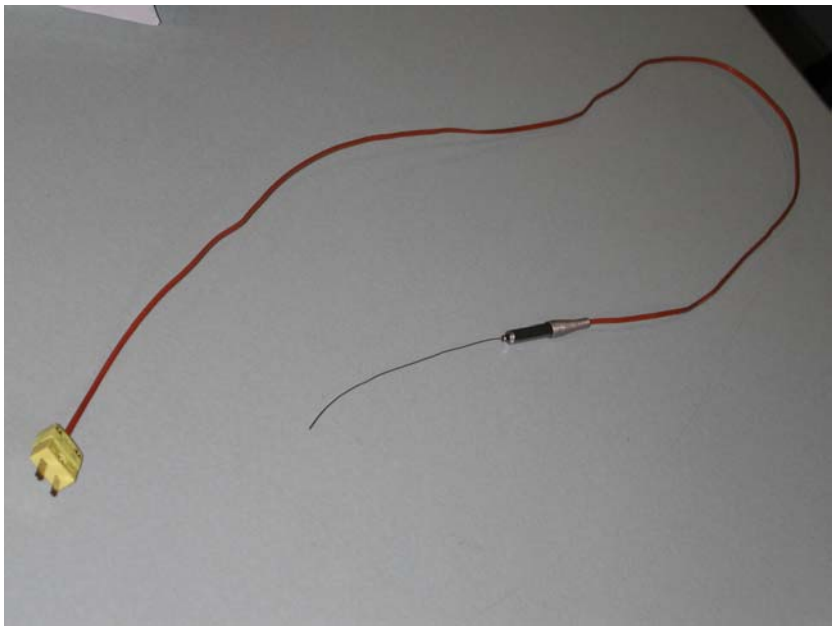

Figure 9. T type Thermocouple.

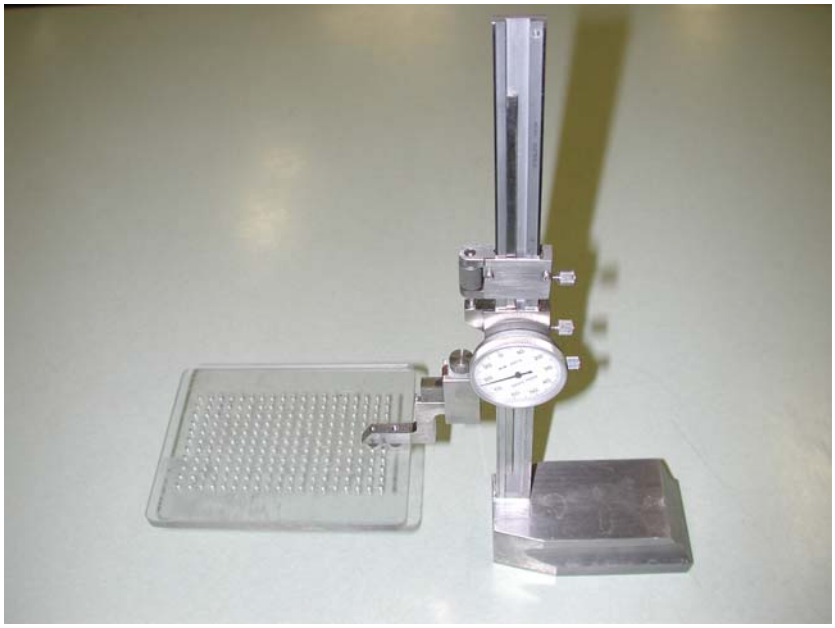

Figure 10. The Dial Height Gauge.

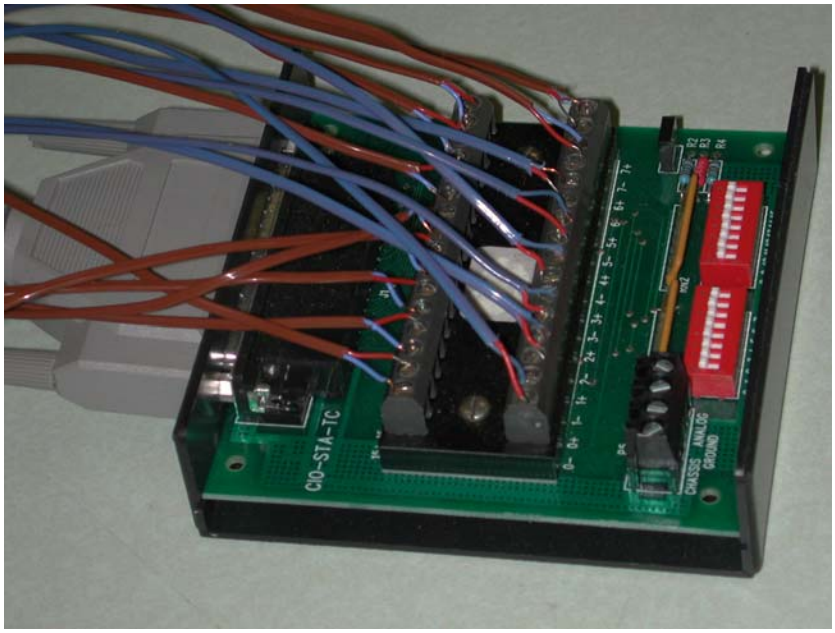

Figure 11. The thermocouple/voltage input Omega data acquisition board.

Figure 12 is the illustration of the IR and laser range imaging system. Specifically, the imaging system contained the following hardware and software components:

- Hardware
    1) Lincoln Impinger Conveyor Oven (Model series 1100);
    2) Indigo uncooled thermal camera with the spectrum range from 7 to 14 microns;
    3) Citizen LCD monitor (Model No. M938-1A);
    4) Host Pentium® IV PC;
    5) Matrox Meteor II image board;
    6) Pulnix red laser line projector;
    7) Pulnix monochromatic CCD camera (TM-6703);
    8) 650nm Corion long-pass filter (LL-650-F);
    9) Matrox Genesis LC board;
    10) Twelve T type TCs;
    11) Dial Height Gauge;
    12) 16-channel thermocouple/voltage input Omega data acquisition board.

- Software

    1) Inspector 2.2 (Matrox Electronics Systems Ltd., Quebec, Canada);

    2) Matlab 6.1 (The Mathworks Inc., MA, USA);

    3) DASwizard (Measurement Computing Corporation, MA, USA).

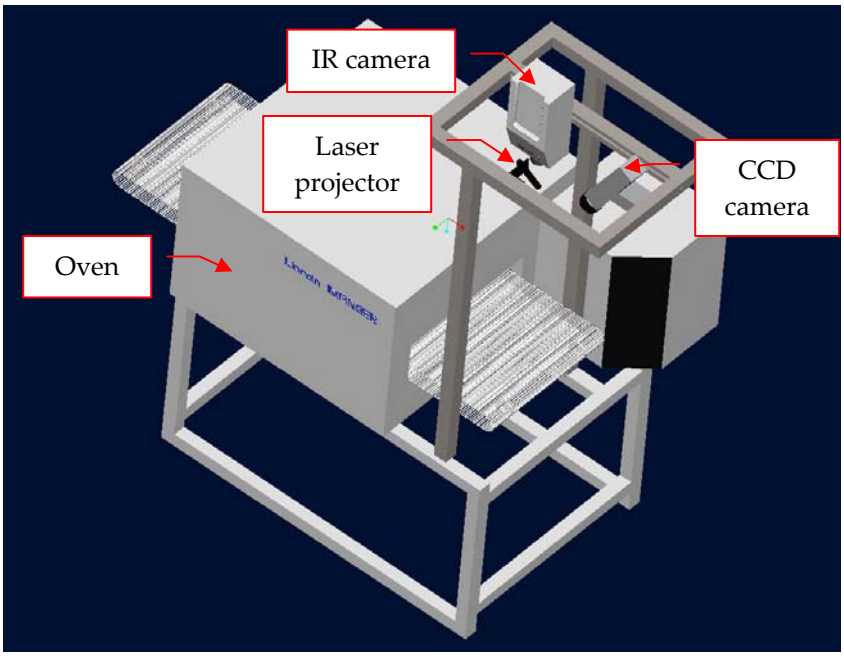

Figure 12. The IR and laser range imaging system.

CHAPTER 5 METHODS

To obtain the mapping relationship between the ANN inputs and outputs, observation data are needed to train and test the ANN estimator. Figure 13 shows the system block diagram. After cooking, chicken samples traveled on the conveyor belt, and sequential IR images were captured to obtain the surface temperature of the chicken breast. Simultaneously, the actual internal temperature was recorded by the embedded TCs. Those temperature pairs were measured for 5 minutes at 10-second intervals. 3D images of the samples were reconstructed by the laser range system to provide thickness and shape information. Then, the external temperature and the geometric information of the sample were input into the ANN to predict the internal cooking temperature. The actual internal cooking temperature acted as a target for the ANN training. Following the training process, the actual internal cooking temperature was compared with the predicted internal cooking temperature. Finally, the system inside the dashed line (see Figure 13) was used to predict the internal cooking temperature in chicken breasts. In addition, the internal cooking temperature estimation system was evaluated using certain evaluation criteria.

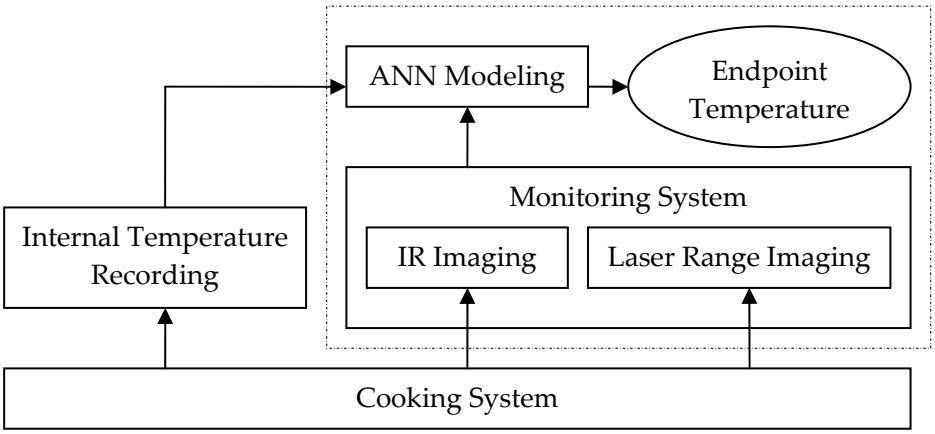

Figure 13. Non-invasive endpoint temperature estimation system.

Essentially there were six stages in this process summarized below and explained in more detail in the following sections.

1. Preparation of samples.
2. System component calibration and adjustment, including TCs linearity test, cooking time setting, IR camera and laser range system setup and calibration.
3. Internal temperature recording.
4. Digital images recording and processing.

   A sequence of IR images was grabbed while the internal temperature of the chicken breast was measured by the TCs after cooking. Meanwhile, 3D images were grabbed using the laser range system. The IR and 3D images were registered to locate the thickest region of the breast. The surface temperature at that region was obtained from

the IR image and the geometric information of the chicken breast was extracted from the 3D image.

5. ANN modeling.

   The modeling had two procedures: training and testing. Model parameters (weights and biases of the ANN) were determined by the ANN training process; that is, plugging recorded surface and internal temperatures and the geometric information into the model to get the parameters using the specific learning algorithm. Following training, the model was tested; the surface temperature and the geometric information were input into the ANN to predict the internal cooking temperature in chicken samples.

6. Discussion of evaluation criteria.

5.1 Preparation of Samples

Boneless and skinless chicken breasts of varied thicknesses and shapes were prepared for this research. The samples were bought directly from major poultry companies on the Eastern Shore without adding any additional water, a solution of chicken broth, or sodium phosphates. To keep the samples fresh, they were refrigerated at 0° C and processed within several days.

The following assumptions were made to simplify the modeling process:

- The ambient temperature and humidity stay constant;
- Chicken breast shrinkage is negligible; and
- The coldest part of the chicken breast is the thickest region.

To reduce the experimental variability, actions were taken as follows:

- Fatty tissues of the chicken breasts were removed and discarded;
- Chicken breasts were cooked without any seasoning;
- The beginning temperature of the chicken breasts was kept constant at 20° C;
- Chicken breasts were placed on the conveyor belt at the same place and the same orientation to avoid skew.

5.2 System Component Calibration and Adjustment

5.2.1 TCs Linearity Test

TCs were used to measure the internal temperature of the chicken breasts in this research. The temperature readings from TCs were treated as "ground truth" values. They were used in two processes. First, during the ANN training process, they were targets to update the ANN parameters. Second, in the

evaluation process, they were compared with the ANN outputs, the predicted internal cooking temperatures, to see how accurately the model was estimating.

The TCs purchased from Omega Company have already been calibrated with an error of ±0.5° C. To test the linearity of the TCs, distilled de-ionized water, a container, and a heat plate were used. The de-ionized water was placed inside the open container and heated to a boil on the heat plate. All twelve TCs were bound together without the probes touching one another. During the cooling process, the TCs were put inside the container and immersed in the water without touching the wall of the container. Temperatures were read every second using the TCs. Each TC reading was the average value within ten seconds. The average reading from the twelve TCs was used as a reference. The TCs were tested at approximately 23, 71, 80, 90, and 100° C, all temperatures within the food processing temperature range.

5.2.2 Cooking Time Setting

In this project, only a constant cooking procedure (cooking time and cooking temperature) was used for comparison among the different input variables to the ANN. Under the specific cooking procedure, the endpoint temperature of the chicken samples was expected for undercooked, perfectly cooked and

overcooked samples. Thus, the dynamic range of the model satisfies the practical application in industry. To find out the proper cooking time for the chicken breast samples, the cooking temperature was set at about 177° C (350° F), because it is the most common cooking temperature in the industry. Then, the middle size chicken samples were cooked at different categories based on their changes with cooking time from 10 to 13 minutes.

5.2.3 IR Camera Setup and Calibration

5.2.3.1 Setup

The IR camera was located above the conveyor platform at a height of 863.6 mm. That specific height was chosen to make the camera as close as possible to the conveyor platform, satisfying the condition that all tested chicken samples were inside the camera field of view. To adjust the camera focus, the lens was regulated until a fine IR image was shown in the LCD monitor. The camera parameter settings are listed in Table 1. The monochrome display mode was preferred for its small data size and simple image processing. To keep the same scale range for all of the IR images, the Auto Gain Control (AGC) function was disabled. Contrast and brightness were set to avoid the saturation of IR images that would lead to a loss of information. The value of emissivity was obtained from the literature (Ibarra et al., 2000). The background temperature is the

ambient temperature of the camera. Here, it was the lab room temperature, which was frequently constant.

Table 1 The specific parameter settings of the IR camera.

Parameters	Value/Status
Display Mode	MONO_G1.0
AGC	Turn off
Contrast	54
Brightness	60
Emissivity	.63
Background Temperature (° C)	25

5.2.3.2 Calibration

In IR images, a lower intensity means a lower surface temperature. The thermograms grabbed by the IR camera only provided intensity information. Therefore, before the experiment, the gray levels of the IR images had to be correlated to actual temperature values.

When the chicken breasts came out of the oven after cooking, IR images were grabbed every second for five minutes. Simultaneously, the TCs in contact with the surface of chicken breasts directly measured the surface temperatures. To reduce error, the surface temperatures for chicken samples were measured in triplicate. The relationship between the intensities of the IR images and the actual temperature values was developed using regression analysis.

5.2.4 Laser Range System Setup and Calibration

The setup for the laser range system is shown in Figure 14. The laser line projector and the CCD camera were mounted on the same stationary frame. The laser projector emitted a red laser line onto the surface of the sample. The laser sheet beam was perpendicular to the conveyor belt platform. The CCD camera, located at 45° from the conveyor belt plane, captured the shifted laser line. When the samples moved with the conveyor belt, the laser line scanned over each sample entirely. The image board connected with the camera grabbed and processed the images.

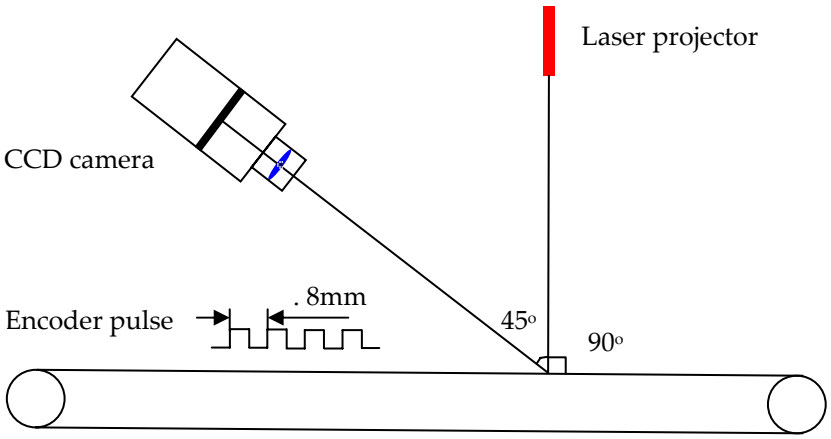

Figure 14. Schematic diagram of laser range system.

In this project, the encoder pulse width was 0.8 mm. The image field width both in the height and width direction was 6" (152.4 mm). Thus, theoretically, the resolutions for the 3D images were: r_L = 0.8 mm, r_h = 0.8 mm, and r_w = 0.2 mm.

The sensor adjustment of laser range system was done by Bio-imaging/Machine Vision Lab at University of Maryland at College Park (Jing, 2003). For the calibration of the system, a known height staircase aluminum block ranged from 5 to 50 mm was prepared. The block was made by a CMM machine. The block was put on the conveyor and scanned several times in the different place on the belt.

5.3 Internal Temperature Recording

Before cooking, each chicken breast was positioned under the height gauge plate. The thickness of each sample was measured by the gauge and a probe was used to mark the thickest part through the pinholes in the plate. As shown in Figure 15, each TC was bent at a 45° angle and the bending length of the probe depended on the thickness of the chicken breast. Based on triangulation, the bending length of the TC probe was calculated as following:

$$L_{TC} = 0.5TH \Big/ \sin 45^{o} = TH \Big/ \sqrt{2} \qquad (10)$$

where L_{TC} is the bending length of a TC probe; TH is the thickness of a chicken breast. The internal temperatures were recorded by inserting TCs at the center of the thickest part of the chicken breasts. As shown in Figure 16, four chicken breasts were cooked at the same time and the internal temperature of each chicken breast was measured in triplicate (see Appendix A). To minimize

variation, the average of the three readings was used. The samples were preheated on the conveyor of the oven. When the internal temperature of the samples warmed up to about 20° C, the samples were moved into the oven, and cooked inside the oven at the predetermined time and temperature.

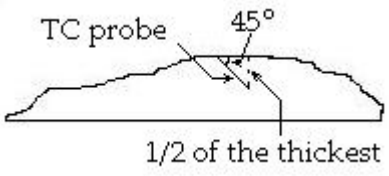

Figure 15. The profile of a chicken sample with embedded TC.

Figure 16. Four chicken breasts before cooking with three TCs inserted into the thickest part of each one.

5.4 Digital Image Recording and Processing

5.4.1 IR Images Grabbing and Processing

The process of grabbing the digital IR images was programmed using the software Inspector 2.2 (see Appendix A). The digitizer settings are given in Table 2.

Following cooking, sequential IR images were grabbed for five minutes at ten-second intervals. First, in each image frame, the four chicken breasts were segmented. Then for each chicken breast, since the thickest part was most likely the coldest area, this part was defined as the region of interest (ROI) in the IR image. To smooth out the variations and noises, the intensity of the ROI was obtained from the average value of an 11 by 11 pixel area whose center was the thickest part. Therefore, the surface temperature of each chicken breast refers to the surface temperature of the ROI.

Table 2 The digitizer control.

Parameters	Value/Status
Input Channel	0 or RCA
Input Region	640 x 480
digitizer	8 bits per channel (4 channels total)
Grab Mode	Synchronous
Setting	RS-170A Monochrome

5.4.2 3D Images Reconstructing and Processing

3D images of the samples were reconstructed by the laser range system to provide thickness and shape (length and width) information. In 3D images, a lower intensity means a thinner breast. The intensity of each pixel corresponds to the thickness information at that pixel position which can be determined by the following equation:

$$TH = \frac{I_{3D}}{4} \tag{11a}$$

where TH (mm) is the thickness of chicken breast; I_{3D} is the pixel intensity of the 3D image; and 4 is the scale factor which is used to calculate the real image size relative to the image in the computer. The length and width information can also be extracted from the 3D image by the following equations:

$$L = C/3 \tag{11b}$$

$$W = R/3 \tag{11c}$$

where L (mm) and W (mm) are the length and width of the chicken breast respectively; C and R are the number of columns and rows in the 3D image, respectively; and 3 is the scale factor.

Each point on the meat surface has a thickness, length and width (see Figure 17), which can be extracted from the 3D image. However, in this research, only the

thickest region was of interest, the longest length and width. Thus, when thickness (TH), length (L) and width (W) are mentioned, they refer to the maximum values of these variables.

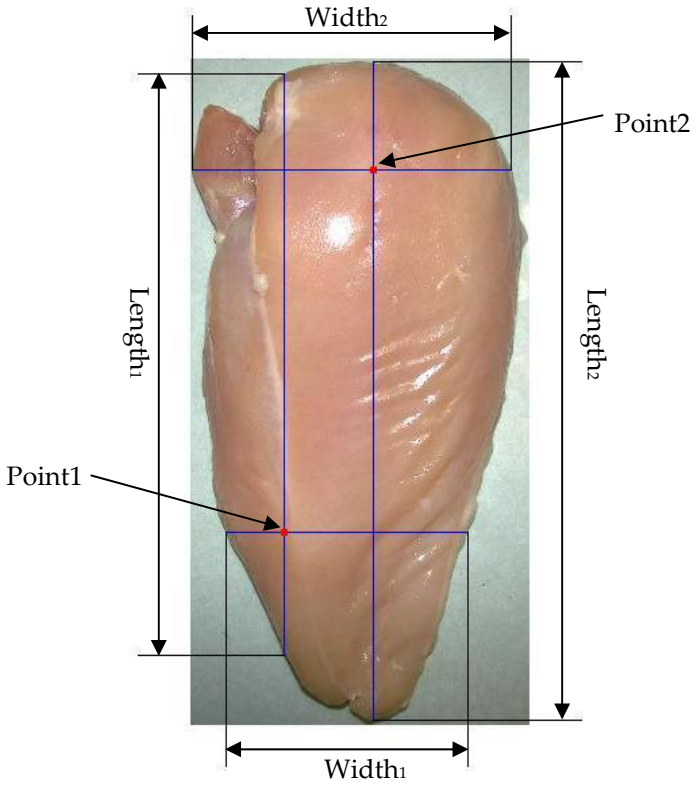

Figure 17. The shape information of a chicken breast.

5.4.3 IR and 3D Images Registration

To obtain the surface temperature of the chicken meat, a ROI was selected in the IR image. Nevertheless, the location of the ROI was achieved by examining the 3D image. Then the surface temperature of the ROI was obtained from the corresponding IR image. The problem was that the IR and 3D images were

different sizes, which meant that in both images the same coordinates did not point to the same position. To identify the location of the ROI in the IR image, both the IR and 3D images had to be registered using the same image scale. In this project, the 3D image was taken as the target size and the IR image was normalized using bicubic interpolation to the same scale as the 3D image. Affine transform was used to register 3D and normalized IR images. Following are the basic ideas of bicubic interpolation (Sonka et al., 1999) and affine transform (Forsyth and Ponce, 2003), respectively:

- Bicubic interpolation

In bicubic interpolation, 16 neighboring pixels are used for interpolation. Given that the size of an original image is W x L and the size of the normalized image (rescaled image) is W′ x L′ (see Figure 18 and 19). Each pixel (i′, j′) in the rescaled image corresponds to a position (x, y) in the original image:

$$\begin{aligned} x &= i'W/W' \\ y &= j'W/W' \end{aligned} \tag{12}$$

$$\begin{aligned} i &= [x] \\ j &= [y] \end{aligned} \tag{13}$$

$$\begin{aligned} dx &= x - i \\ dy &= y - j \end{aligned} \tag{14}$$

x, y could be non-integer. For digital images, each pixel coordinates have to be integers. So i and j are the integer part of x and y, respectively. The intensity value of pixel (i', j') in the rescaled image is

$$I(i', j') = \sum_{m=-1}^{2} \sum_{n=-1}^{2} I(i+m, j+n) R(m-dx) R(dy-n) \tag{15}$$

The weighting function R(x) is

$$R(x) = \frac{1}{6}\left[P^3(x+2) - 4P^3(x+1) + 6P^3(x) - 4P^3(x-1)\right]$$
$$P(x) = \begin{cases} x & x > 0 \\ 0 & x \le 0 \end{cases} \tag{16}$$

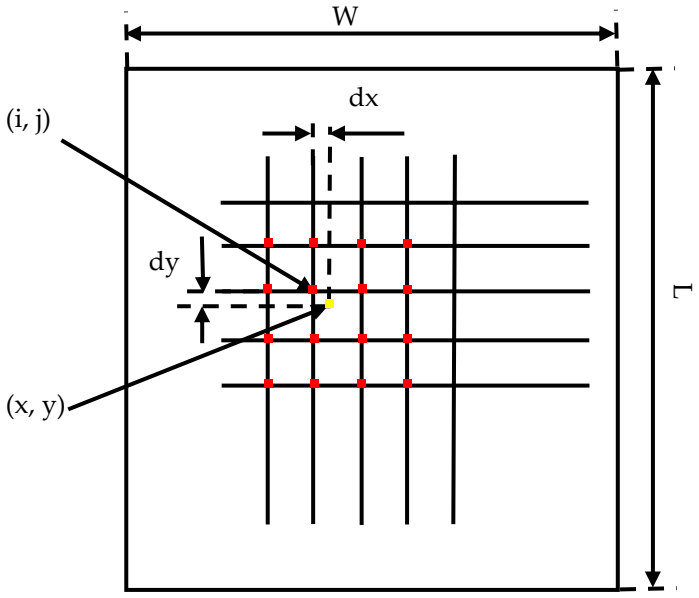

Figure 18. The original image.

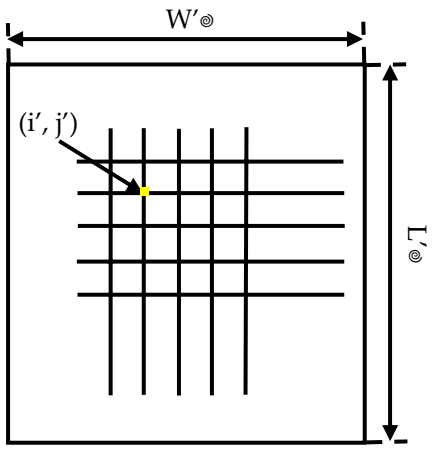

Figure 19. The normalized image.

- Affine transform

Affine transform is a linear transformation between two images based on following equations:

$$\begin{aligned} i' &= ai + bj + c \\ j' &= di + ej + f \end{aligned} \tag{17}$$

or in matrix notation:

$$\begin{bmatrix} i' \\ j' \end{bmatrix} = \begin{bmatrix} a & b & c \\ d & e & f \end{bmatrix} \times \begin{bmatrix} i \\ j \\ 1 \end{bmatrix} \tag{18}$$

where (i, j) and (i', j') are the coordinates in two images, respectively; a and e are scaling factors; b and d are rotation factors; and c and f are translation factors. In this research, only scaling and translation need to be considered when IR and 3D images were registered. Thus the transformation simplified to:

$$\begin{bmatrix} i' \\ j' \end{bmatrix} = \begin{bmatrix} a & 0 & c \\ 0 & e & f \end{bmatrix} \times \begin{bmatrix} i \\ j \\ 1 \end{bmatrix} \tag{19}$$

And only two sets of [i', j', i, j] are required to solve this equation.

5.5 ANN Modeling

A 4-10-1 MLP ANN, as shown in Figure 20, was developed to model the nonlinear heat transfer process and to predict the internal cooking temperature of the chicken breasts. The input variables were external temperature, thickness, length, and width of each sample. External temperature was denoted as ET(0 + nΔ), (0 ≤n ≤ 29, Δ = 10 seconds), where n is the lag number. ET(0) revealed the surface temperature of the sample immediately out of the oven, while ET(nΔ) was the temperature after the nΔ time delay. The actual internal temperature was the target during the ANN training, that is, the output of the ANN was the predicted internal temperature of each sample. To get a better performance of the ANN, all of the input variables and targets were normalized by the following equation so that they would always fall between 0 and 1:

$$V_{norm} = \frac{V - V_{\min}}{V_{\max} - V_{\min}} \tag{20}$$

Where V is the original variable value; V_{min}, V_{max} and V_{norm} are the minimum, maximum and normalized values of V, respectively. Thus, the input vector was

[ET(0 + nΔ)$_{norm}$, TH$_{norm}$, L$_{norm}$, W$_{norm}$]′. The transfer function between each layer is the log-sigmoid function defined as (Hagan et al., 1995)

$$\sigma = \frac{1}{1+e^{-x}} \tag{21}$$

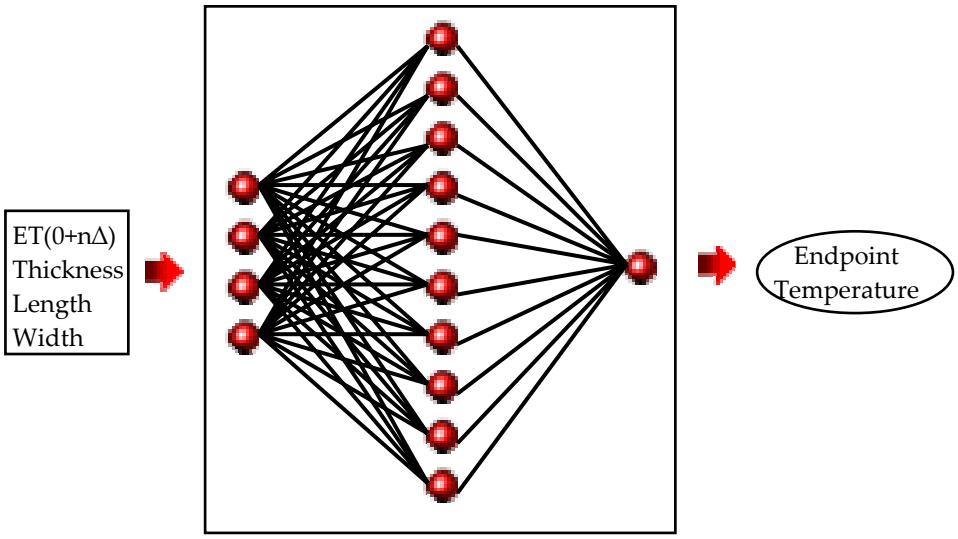

Figure 20. The 4-10-1 MLP ANN architecture.

The Gauss-Newton approximation to Bayesian regularization (GNBR) algorithm was used to train the network. The algorithm trains the network by minimizing the following performance function (Foresee and Hagan, 1997):

$$F = \beta E_E + \alpha E_W \tag{22}$$

Where α and β are coefficients; E$_E$ is the sum of squares of the error (SSE); E$_W$ is the sum of squares of the network weights (SSW). This is an improvement over the LM algorithm because its performance function considers not only the SSE, but also the associated network weight values (SSW). This function makes the

response of the network smoother (Foresee and Hagan, 1977). Nevertheless, the GNBR algorithm still incorporates the LM algorithm to minimize the performance function (equation 22).

The LM algorithm uses the following equations to update the weights and biases of the network:

$$\Delta X_k = -\left[J^T(X_k)J(X_k) + \mu_k I\right]^{-1} J^T(X_k)V(X_k) \tag{23a}$$

$$J(X) = \begin{bmatrix} \frac{\partial V_1(X)}{\partial x_1} & \frac{\partial V_1(X)}{\partial x_2} & \cdots & \frac{\partial V_1(X)}{\partial x_n} \\ \frac{\partial V_2(X)}{\partial x_1} & \frac{\partial V_2(X)}{\partial x_2} & \cdots & \frac{\partial V_2(X)}{\partial x_n} \\ \vdots & \vdots & & \vdots \\ \frac{\partial V_N(X)}{\partial x_1} & \frac{\partial V_N(X)}{\partial x_2} & \cdots & \frac{\partial V_N(X)}{\partial x_n} \end{bmatrix} \tag{23b}$$

Where J is the Jacobian Matrix; N is the number of observations; V(X) is an N x 1 error vector; X is composed of weights and biases; μ is a constant; I is an identity matrix; and ΔX_k is the increasement of weights and biases and k means in the k^{th} iteration.

The steps of the LM algorithm are as follows (Hagan et al., 1995):

1. Initialize the weights, biases and μ_k of the network;
2. Input all of the training data into the network and calculate the outputs and the SSE;

3. Calculate the Jacobian matrix by equation 23b;
4. Solve the function 23a to obtain ΔX_k;
5. Recalculate the SSE using $X_k + \Delta X_k$. If the recalculated SSE value obtained in this step is less than the original SSE, then μ_k is divided by a constant (usually 10), letting $X_{k+1} = X_k + \Delta X_k$. Then training data are input again from step 2 with the new X_{k+1} value. If the recalculated SSE value is greater than the original SSE value then μ_k is multipled by a constant (usually 10) and the process is repeated from step 4 again. Reiterate until the performance goal is reached.

The steps of the GNBR algorithm are as follows (Foresee and Hagan, 1997):

1. Initialize α, β and weights and biases;
2. Input all the training data to the network and calculate the outputs and the SSE and SSW;
3. Use the LM algorithm to minimize the performance function;
4. Compute the effective number of parameters γ;
5. Update $\alpha = \frac{\gamma}{2E_W(W)}$ and $\beta = \frac{n-\gamma}{2E_E(W)}$, where n is the total number of observations;
6. Iterate steps 2 through 5 until convergence is achieved.

For more details about the LM and GNBR algorithms, see references (Hagan and Menhaj, 1994; Thodberg, 1996).

5.6 Discussion of Evaluation Criteria

To compare the effect of different lags and different geometric information on the ANN performance, the following measurements were used as criteria:

- Mean square error (MSE)

$$MSE = \frac{\sum_{i=1}^{N}\left(IT_{ANN\,i} - IT_{TC\,i}\right)^2}{N} \tag{24a}$$

- Mean absolute error (MAE)

$$MAE = \frac{\sum_{i=1}^{N}\left|IT_{ANN\,i} - IT_{TC\,i}\right|}{N} \tag{24b}$$

- Mean absolute percent error (MAPE)

$$MAPE = \frac{\sum_{i=1}^{N}\left|\left(IT_{ANN_i} - IT_{TC_i}\right)/IT_{TC_i}\right|}{N} \tag{24c}$$

Where IT_{ANN_i} is the predicted internal cooking temperature from the ANN output; $IT_{TC\,i}$ is the actual internal cooking temperature measured by the TCs embedded in the chicken breast samples. N is the number of observations.

CHAPTER 6 RESULTS AND DISCUSSION

In this chapter, the experimental results are reported first. Then, the ANN estimator accuracy and the effects of different surface temperature lags and 3D information on the ANN performance are discussed.

6.1 System Component Calibration and Adjustment Results

6.1.1 TCs Linearity

Twelve TCs were tested within the food processing temperature range. The results are shown in Table 3 and Figure 21 illustrates the regression relationship between readings of TC #1 and reference values. For TC #2 through TC #12, the corresponding regression illustrations are similar to that of TC #1 (see Appendix B). The test results show that the TCs proved to be linear within the experiment required temperature range.

Table 3 Average temperature readings (° C) within ten seconds from each TC.

TC	Test Points at about				
	23	**71**	**80**	**90**	**100**
1	23.02[a]	71.42	80.28	90.22	100.20
2	22.84	71.46	80.10	89.94	100.11
3	23.01	71.31	79.83	89.53	99.27
4	22.85	71.40	79.99	90.05	100.02
5	22.78	71.28	79.94	89.81	99.81
6	23.15	71.04	79.70	89.70	99.51
7	22.82	71.36	79.90	89.71	99.77
8	23.01	71.35	79.80	89.72	99.71
9	22.97	71.57	80.20	90.11	100.05
10	22.89	71.45	80.10	89.98	99.78
11	23.07	71.29	79.97	89.85	99.75
12	22.87	71.46	79.99	89.96	99.93
Mean[b]	**22.94**	**71.37**	**79.98**	**89.88**	**99.82**

Note:

a: Each value is the average value of ten temperature readings for ten seconds at 1-second intervals.

b: The mean is the average of the column values. It is treated as reference to compare with values of each TC.

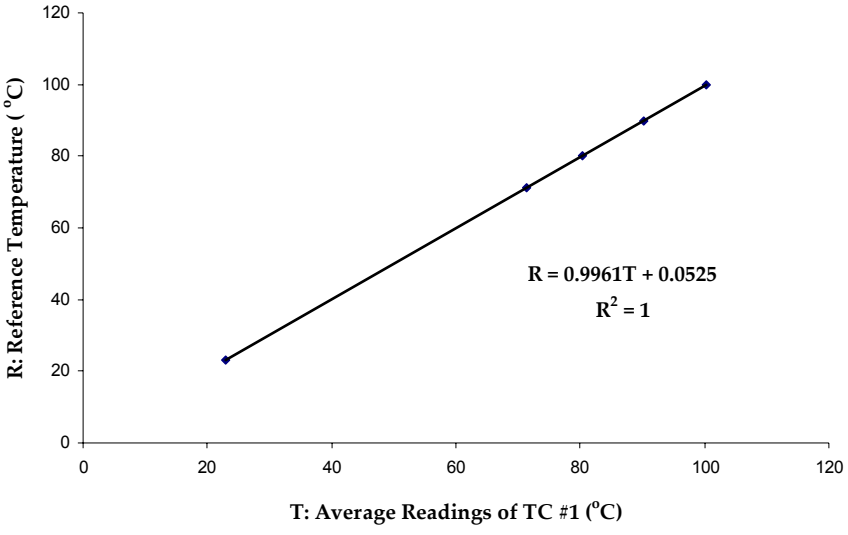

Figure 21. Linearity test of TC #1.

6.1.2 Cooking Time

Sixteen mid-size chicken breasts were used to assess the endpoint temperature under different cooking times. Four cooking times: 10, 11, 12, and 13 minutes, were tested in quadruplicate. The cooking temperature was 177° C. Table 4 shows the results and the mean value was used as a standard to choose the appropriate cooking time. Based on the USDA's regulation (76.7° C for chicken breasts), the mean value for thirteen minutes was the closest to the requirement and thirteen minutes was the optimum choice. Thus, in this research, all experiments were performed at 177° C cooking temperature and a cooking time of 13 minutes.

Table 4 Internal cooking temperature (° C) for test samples.

Cooking Time (minutes)	Sample 1	Sample 2	Sample 3	Sample 4	Mean[a]
10	62.8	64.8	64.6	60.6	63.2
11	73.4	75.8	79.9	62.1	72.8
12	64.5	76.8	78.3	73.8	73.4
13	79.7	84.9	74.9	72.0	77.9

a: The mean is the average of the row values.

6.1.3 IR Camera

After cooking, the surface temperature of each chicken breast was measured by TCs in triplicate. Meanwhile, IR images were grabbed at an interval of one second for five minutes. Using regression analysis, the experiment showed that

the relationship between the intensity of the IR images and the surface temperature is defined as equation 25, and is shown in Figure 22.

$$ET = 0.1925\, I_{IR} + 46.415 \qquad (25)$$

where ET (° C) is the surface temperature; and I_{IR} is the average intensity of the ROI in the image. Following the experiment, the surface temperatures were calculated from the intensity of the IR images based on this equation.

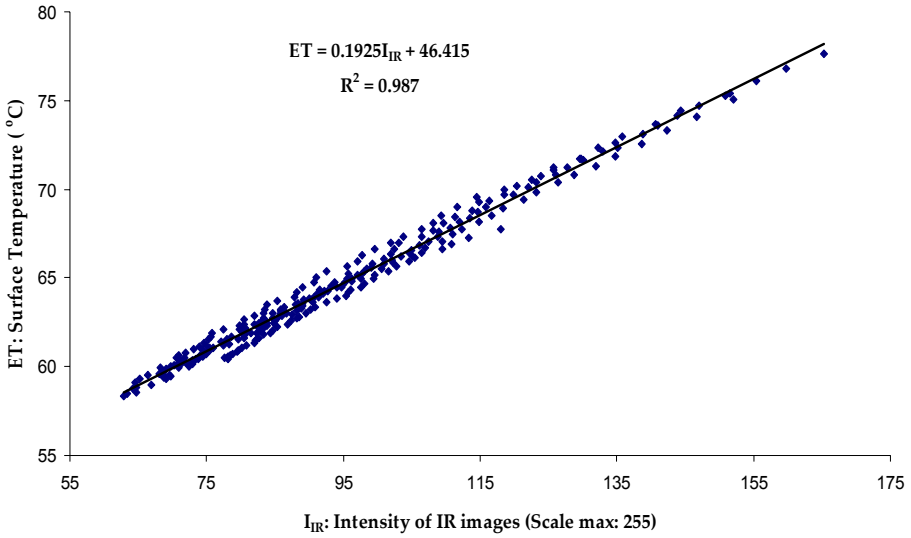

Figure 22. The relationship between the intensity of IR images and surface temperature in chicken breasts (275 data from 6 sampling points in meats).

6.1.4 Laser Range System

The calibration of laser range system was done by Bio-imaging/Machine Vision Lab at University of Maryland at College Park (Jing, 2003). The known height staircase block was scanned several times by using the system in the different

place on the conveyor belt. The calibration results are shown in Table 5. From Table 5, the calibration precision was enough to produce satisfactory accuracy.

Table 5 Laser range system calibration result (mm).

Actual thickness[a]	Measured thickness		
	Mean	Error	Standard deviation
5	4.84	-0.16	0.03
10	9.74	-0.26	0.02
15	14.77	-0.23	0.03
20	19.97	-0.03	0.04
25	24.99	-0.01	0.02
30	30.23	0.23	0.03
35	35.29	0.29	0.03
40	40.14	0.14	0.03
45	45.00	-0.00	0.03
50	50.01	0.01	0.03

a: The staircase block was made by a CMM machine with the range from 5 to 50 mm in 5 mm increments. The tolerance for the actual thickness is ±0.0254 mm (±1/1000 inch).

6.2 Cooking and Cooling Processes

Chicken breasts were cooked for 13 minutes at 177° C and cooled down on the conveyor belt for five minutes. During the experimental process, the room, and internal and external temperatures in chicken breasts were monitored using TCs. Figure 23 shows the graph of these temperatures. The room temperature was almost constant during the experiment. In the cooking phase, the internal temperature of the chicken samples increased gradually, while the surface temperature fluctuated as it increased. Heat transfer in chicken meat is non-

homogeneous. Although all kinds of heat transfer are dependent on a temperature gradient, the thermal process is complex in chicken breasts during heating. The reason is that during heating, many physical and chemical changes occur in the chicken breast. Also, the heating pattern, such as one side or two sides heating, affects the heat transfer process. Instead of the heating phase, in this research, the internal cooking temperature was estimated during the cooling phase.

Figure 24 shows how the internal and external temperatures changed in the chicken breasts during the cooling phase. With the specific cooking procedure, whether the chicken samples were overcooked, perfectly cooked or undercooked, initially the internal temperature increased slightly and then decreased gradually, while the external temperature decreased immediately and faster than the internal temperature. Generally, if only the internal and surface temperatures were considered, there were two different heat transfer stages in the cooling phase (see Figure 25). Immediately after cooking, heat still propagated from the surface into the center of the meat sample and at the same time the meat surface lost heat to the ambient air. In addition, after the chicken breast temperature reached thermal equilibrium, heat was transferred from the inside to the outside of the chicken and then dispersed into the ambient air.

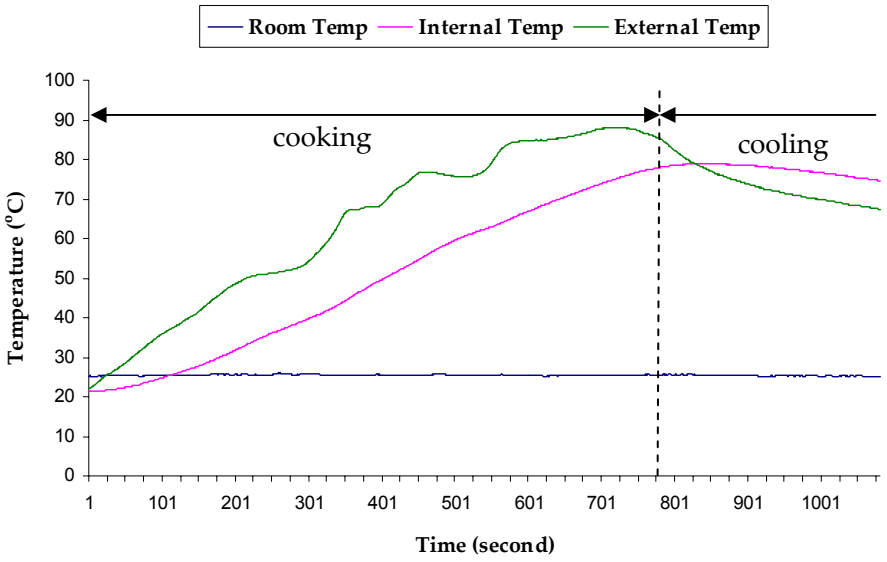

Figure 23. Typical temperature readings in cooking and cooling processes.

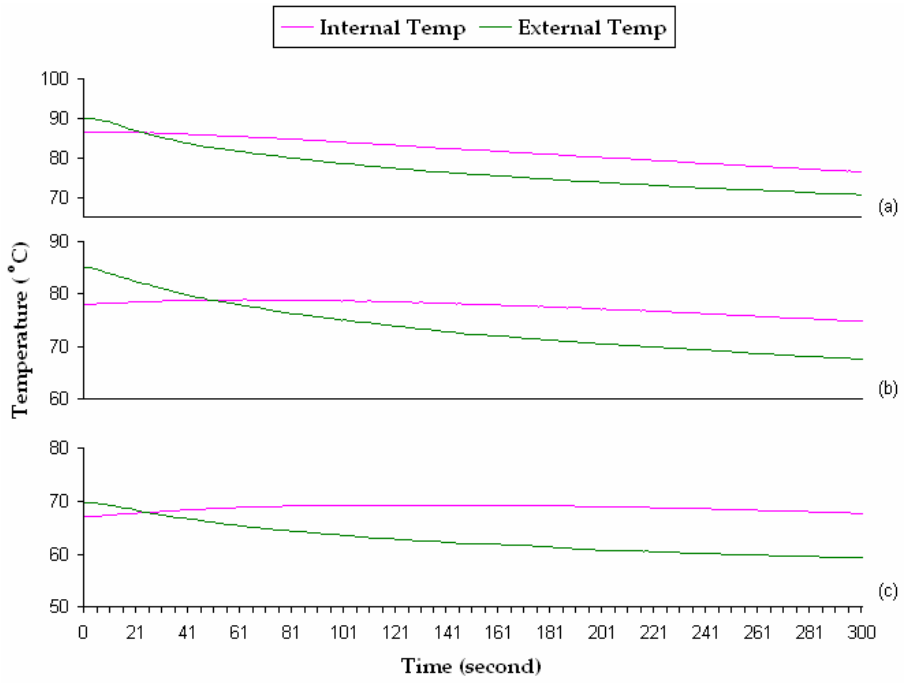

Figure 24. Typical internal and external temperature readings in cooling process: (a) overcooked chicken sample; (b) well-cooked sample; and (c) undercooked sample.

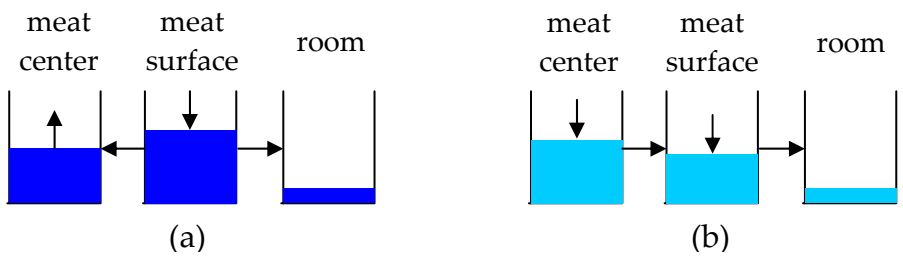

Figure 25. Schematic diagrams of two heat transfer processes during the cooling phase using water flow among the tanks analogous to heat flow in the chicken breast: (a) before heat reached equilibrium in chicken breast; and (b) after the equilibrium. The horizontal arrow indicates the direction of heat flow and the perpendicular arrow indicates the direction of temperature changes.

6.3 IR and 3D Images Processing

Figure 26 shows an IR image of four chicken breasts and a sequence of similar images was grabbed each second for five minutes after heating. For one segmented chicken breast, the sequential thermal images are shown in Figure 27a and b. The intensity index (on the left side of Figure 27a) was obtained based on equation 25. Figure 28a shows the reconstructed 3D image of the chicken breast. In 3D images, a less intense area is a thinner area. The values for thickness, length, and width of the chicken breast were extracted from the 3D image according to equations 11 a, b, and c.

Since the size of the IR image was smaller than the 3D image, the IR image was normalized to the same scale as the corresponding 3D image by using bicubic interpolation (see Figure 28b). Furthermore, the ROI was selected in the 3D

image and mapped into the corresponding IR image as shown in Figures 28c and d. The surface temperature of the ROI was the average value of the 11 by 11 pixel area (inside the green squares in Figure 28d). Additional 3D and normalized IR images are shown in Appendix C.

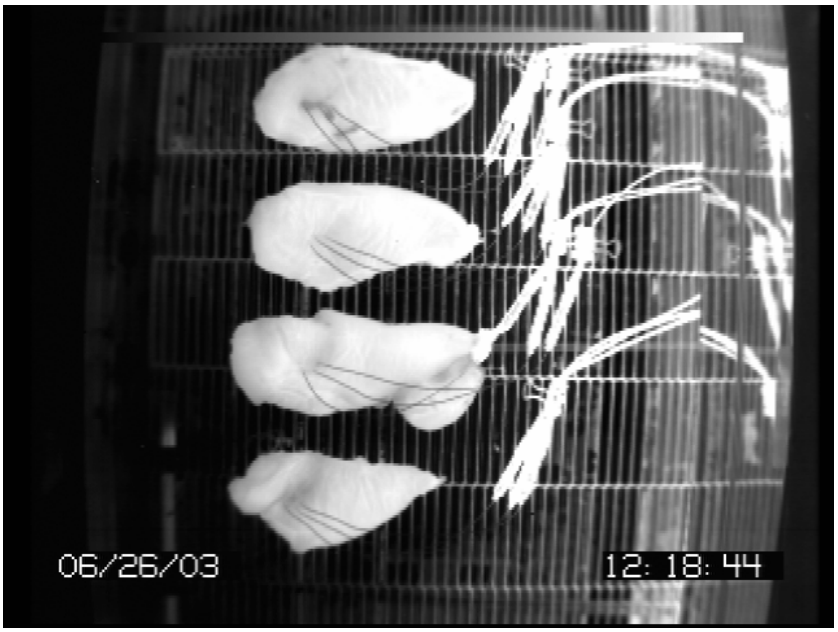

Figure 26. A typical thermal image of cooked chicken breasts.

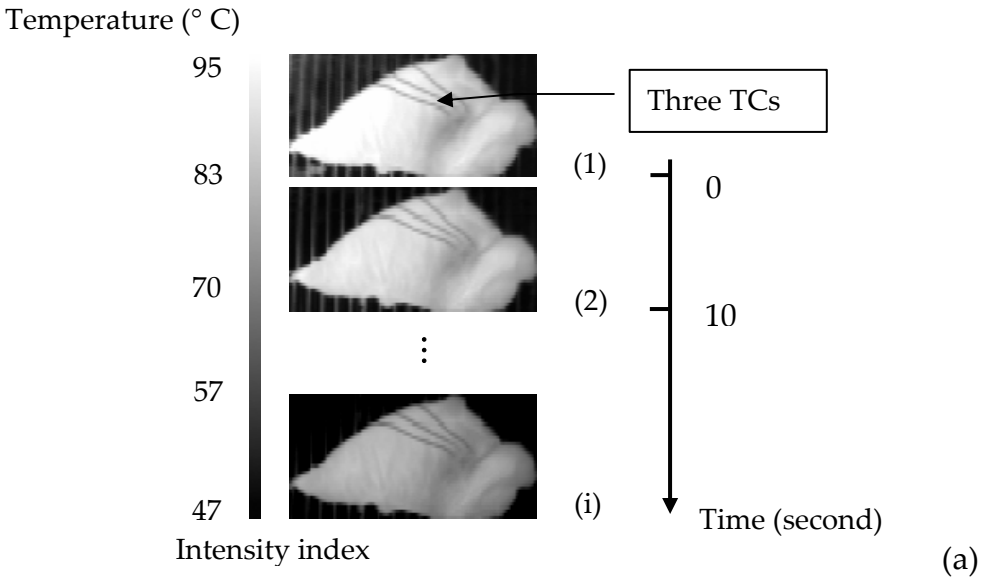

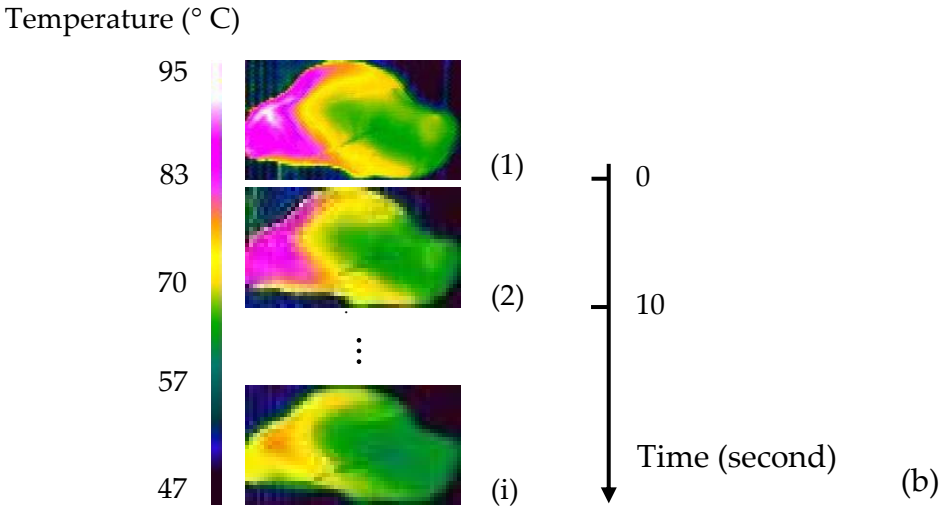

Figure 27. (a) Sequential IR images of a chicken breast grabbed post cooking in the monochrome mode: (1) Immediately; (2) after 10 seconds; and (i) after (i-1) x 10 seconds. (b) Sequential IR images in pseudo color mode.

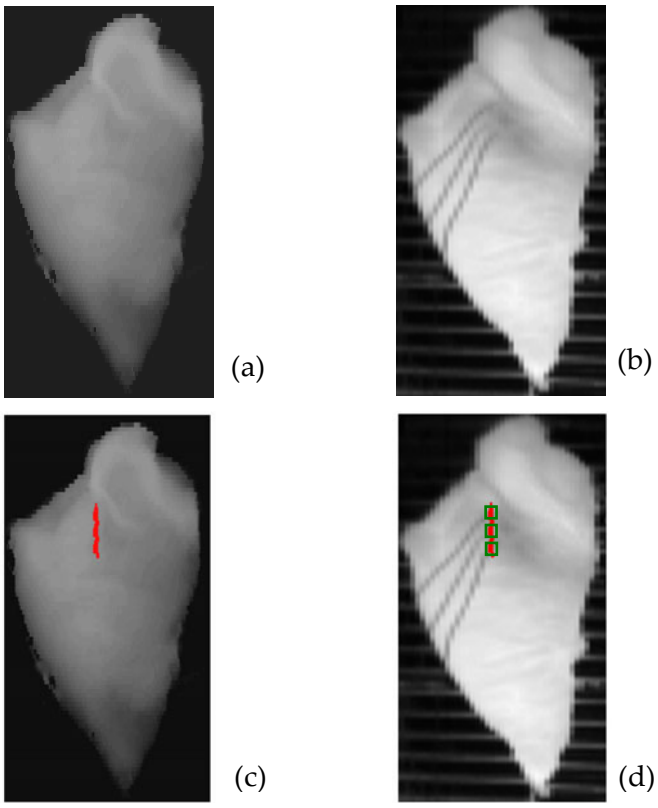

Figure 28. (a) The 3D image of a chicken breast; (b) the corresponding resized IR image; (c) ROI (red region) was located in the 3D image; (d) the ROI was mapped into the corresponding IR image. Each green square is an 11 by 11 pixel area selected to smooth out noises and variations (1 pixel size = .7 x .7 mm^2).

6.4 ANN Estimator Accuracy Test

In this study, 85 boneless chicken breasts of varied thicknesses and shapes were cooked. The 85 breasts were split into two sets: a training set and a test set. Fifty-nine breasts were used for training the ANN, and the other 26 breasts were used for testing.

First, the capacity of the ANN estimator was tested. The external temperature with three lags (ET(nΔ), ($0 \le n \le 2$, $\Delta = 10$ seconds)) and the geometric information of the chicken samples were used as the ANN inputs. The range of the ANN input variables are given in Table 6. Following was one example of initial weights and biases used in the training process:

$$W_1 = \begin{bmatrix} -3.9832 & 4.2675 & -2.1903 & -2.3646 & 2.1984 & -3.2795 \\ -4.1119 & 1.9947 & 2.5487 & 0.5064 & 4.3971 & 4.0891 \\ -3.5114 & -4.8474 & -2.0587 & -3.8366 & -1.3011 & 1.3526 \\ -4.8204 & 3.3217 & -0.5777 & -0.4139 & 5.2788 & -1.4116 \end{bmatrix}$$

$$b_1 = \begin{bmatrix} 5.7912 \\ -3.7014 \\ 5.8870 \\ -4.7007 \end{bmatrix}$$

$$W_2 = \begin{bmatrix} -4.7272 & -3.8138 & -5.0316 & 6.0795 \\ -3.7703 & -7.0924 & -5.7701 & -1.1652 \\ 5.4295 & -7.2067 & -3.3130 & 2.6034 \\ 0.0762 & 7.1567 & 3.6217 & -5.9015 \\ 3.7557 & -0.3682 & -3.1805 & -8.6494 \\ -4.1650 & 6.0871 & -5.2240 & 4.1807 \\ -5.4501 & -5.1818 & -5.1533 & 4.0072 \\ -4.8846 & 3.1777 & 4.1211 & 6.9447 \\ 4.7292 & 4.6444 & 3.7053 & -6.4423 \\ -2.4391 & -2.0372 & -9.2675 & -1.7843 \end{bmatrix}$$

$$b_2 = \begin{bmatrix} 8.7257 \\ 12.7717 \\ -1.5228 \\ -4.1363 \\ 3.6679 \\ -0.9926 \\ 4.2293 \\ -7.4457 \\ 0.5544 \\ 2.7848 \end{bmatrix}$$

$$W_3 = \begin{bmatrix} 1.6575 & 3.1288 & -2.5917 & -0.9288 & 1.5835 & -0.9822 & 0.4382 & 1.1327 & 2.0974 & 1.3774 \end{bmatrix}$$

$b_3 = -3.4563$.

Following training, the adjusted weights and bias were:

$$W_1 = \begin{bmatrix} 3.1785 & -0.9306 & -3.1253 & 4.7694 & 1.4155 & -3.5984 \\ -2.8556 & 2.4084 & 1.5582 & 1.1167 & 1.4440 & 2.6330 \\ -4.7651 & -4.2768 & -3.0630 & 0.4324 & 0.5512 & 0.7207 \\ 3.7375 & -4.6651 & -5.9163 & 1.4575 & 0.6360 & 0.1051 \end{bmatrix}$$

$$b_1 = \begin{bmatrix} -1.7726 \\ -4.5011 \\ 1.0650 \\ 3.6348 \end{bmatrix}$$

$$W_2 = \begin{bmatrix} 1.9708 & -0.4286 & -0.3071 & -0.2254 \\ 1.5202 & -0.3006 & -0.1953 & -0.3652 \\ 2.0110 & -0.4294 & -0.2959 & -0.1938 \\ 8.2766 & -3.8753 & -5.3473 & -3.1226 \\ 1.2972 & -0.2342 & -0.1111 & -0.3531 \\ -1.5598 & 0.3218 & 0.2144 & 0.3918 \\ -0.9081 & 0.1250 & -0.0107 & 0.2545 \\ -1.2279 & 0.2104 & 0.0705 & 0.3438 \\ 1.1194 & -0.1804 & -0.0474 & -0.3129 \\ -0.6955 & 0.0774 & -0.0346 & 0.1809 \end{bmatrix}$$

$$b_2 = \begin{bmatrix} 0.0091 \\ -0.0751 \\ 0.0386 \\ -0.9342 \\ -0.0917 \\ 0.0899 \\ 0.0783 \\ 0.0949 \\ -0.0883 \\ 0.0556 \end{bmatrix}$$

$$W_3 = \begin{bmatrix} 1.9825 & 1.6013 & 2.0049 & -8.8789 & 1.3744 & -1.7281 & -1.0142 & -1.3709 & 1.1782 & -0.7771 \end{bmatrix}$$

$b_3 = -0.1200.$

Figures 29 and 30 show the ANN estimation results for the training and test data sets, respectively. The coordinates of each data point in each diagram represent the actual and predicted temperature pairs. A diagonal dotted line (A = P) means a perfect match between the predicted and actual internal cooking temperatures, which is called line identity. The regression lines are also shown in Figures 29 and 30.

Table 6 The 85 cooked sample properties used in this study for testing the performance of the IR and laser range imaging system.

Parameter	Range
External temperature (° C)	66.6 - 90.6
Thickness (mm)	9.3 - 19.5
Length (mm)	54.7 - 130.7
Width (mm)	37.7 - 90.7

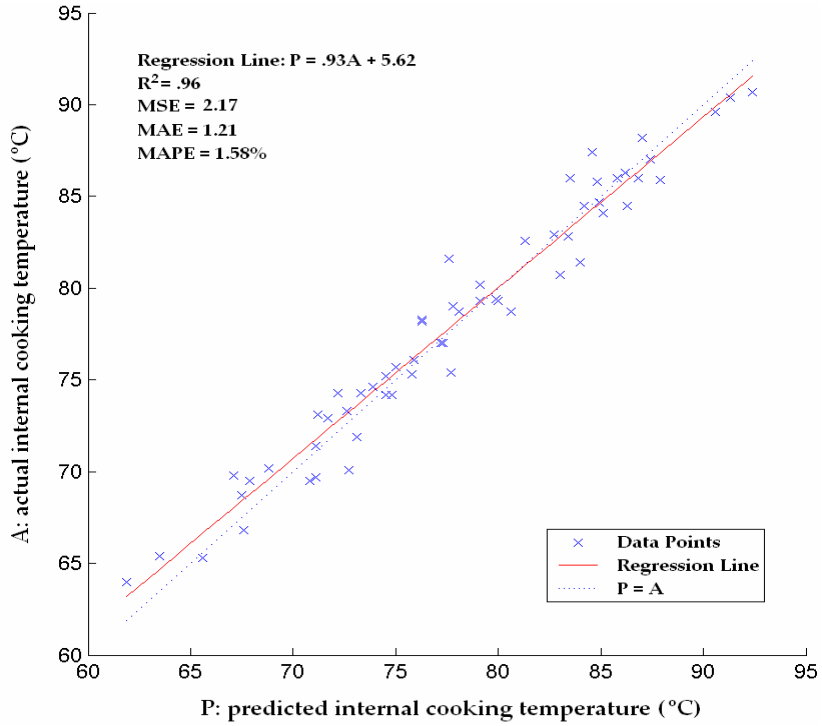

Figure 29. Comparison between the measured and predicted internal cooking temperature for training set (59 samples).

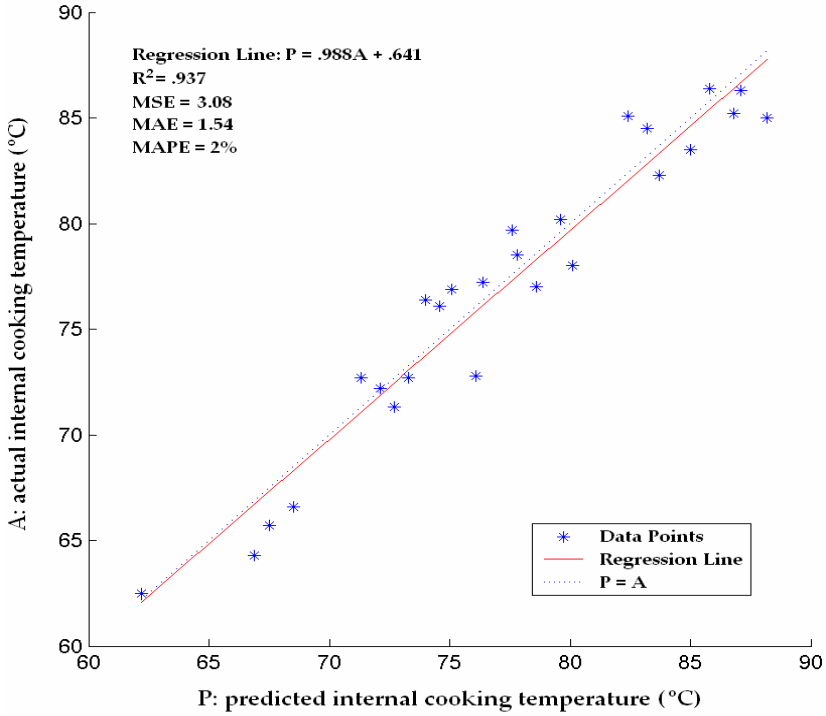

Figure 30. Comparison between the measured and predicted internal cooking temperature for test set (26 samples).

6.5 Impact of Different Lags on ANN Performance

In the industry, the speed of the conveyor belt is 2 feet/second (609.6 mm/second), requiring real-time temperature estimation. As a nonlinear mapping process, the ANN needs more data for accuracy. To trade off between both factors the ANN performance was studied under different lag inputs.

The surface temperature with n lags, denoted as time series ET(0), ET(1Δ), ET(2Δ), …, ET(nΔ), ($0 \leq n \leq 29$, $\Delta = 10$ seconds), were chosen to predict the internal cooking temperature. For instance, n = 0 means that only the instant surface temperature was used to predict the endpoint temperature; while n = 1 means both ET(0) and ET(10) were used to predict the endpoint temperature. To find the optimal number of lags for estimating the internal cooking temperature, one to four lags were used in the experiment. The test results are shown in Table 7. From one to three lags, MAE and MAPE changes were considered insignificant, and the MSE dropped consistently. However, with four lags, the ANN performance did not improve at all, since with more lags, the heat transfer process changed from the first stage to the second stage and more heat was lost to the ambient air. Also, more noise was introduced to the ANN mapping function.

Table 7 Prediction accuracy of the ANN for different lags (26 samples).

	1 Lag n = 0	2 Lags n = 1	3 Lags n = 2	4 Lags n = 3
MSE	3.73	3.14	3.08	4.58
MAE	1.56	1.54	1.54	1.77
MAPE	2%	1.98%	2%	2.25%

According to the testing, the input with three lags was preferred in terms of MSE criteria. No significant improvement was found according to other criteria. This is probably due to the magnification effect of MSE so that a tiny performance difference could be detected. Although it seems reasonable to argue that one lag was much faster and more convenient to implement, it only provided partial heat transfer information compared with using three lags. Three lags were preferred in this estimation system, especially for inspecting meats under a changing cooking procedure. Using three lags contained much more information about the heat transfer process during the cooling phase. In other cases, such as a relatively constant cooking procedure, one lag was a better choice.

6.6 Impact of Different Geometric Information on ANN Performance

Each input variable of the ANN had its own contribution to predicting the endpoint temperature. In this experiment, four categories of input variables were compared. They were as follows:

- ET, the input only included the external temperature with three lags;
- ET, L and W, the external temperature, and shape information (length and width) were added into the inputs;
- ET and TH, the external temperature and thickness information were added into the inputs;
- ET, TH, L and W, the external temperature, shape and thickness information were considered.

The effect on the ANN performance of using different combinations of inputs for the test set is shown in Figure 31. The experimental results are labeled on top of each bar diagram. If the ET was the only input, the laser range system was not required. From this diagram, it can be seen that based on all criteria, the estimation error dropped consistently when additional geometric information was added. For the experiment with the most geometric information, the ANN prediction gave the best performance, and the accuracy

improved from 5.72% to 2% for the MAPE and from 24.7 to 3.08 (° C)^2 for the MSE. On the other hand, thickness information played a more important role than the width and length information. However, using thickness alone was still not enough to produce satisfactory prediction accuracy (± 1° C).

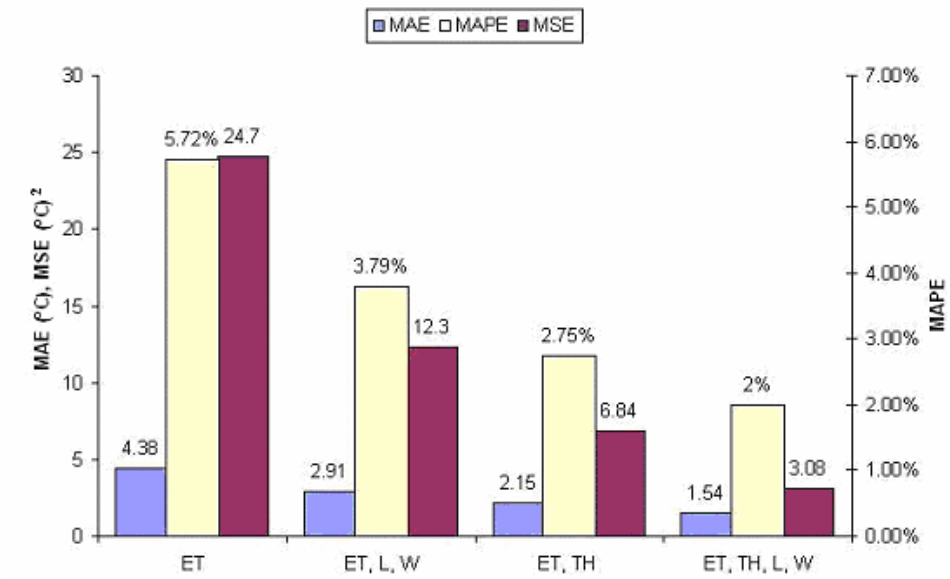

Figure 31. Effect of geometric information on the ANN performance in test set (MSE: mean square error; MAE: mean absolute error; and MAPE: mean absolute percent error).

CHAPTER 7 CONCLUSIONS

A non-invasive internal cooking temperature estimation system was presented in this research. The experimental results showed that geometric information about the chicken breast played a crucial role in internal cooking temperature estimation as well as the surface temperature, which indicated that only relying on IR imaging was not sufficient to get a good estimation. It was necessary to couple laser range imaging with IR imaging.

Moreover, with 3D information and three surface temperature lags as the ANN inputs, the optimal accuracy achieved by this system was 1.54° C for the MAE, 2% for the MAPE, and 3.08 (° C)^2 for the MSE. However, it still has not reached the satisfactory prediction accuracy. The acceptable prediction error is ±1° C based on USDA's goal. Finally, in this research, the required time for the estimation was significantly shortened to 20 seconds making on-line estimation possible. Nevertheless, the temperature estimation system required expensive equipment (see Appendix D).

The combined IR and laser range imaging system shows great potential for real-time, non-contact, and non-invasive estimation of the internal cooking temperature in meat for enhanced food quality and safety.

CHAPTER 8 SUGGESTIONS FOR FURTHER STUDY

In this ANN model, only the length and the width of the chicken samples are taken into account as the "shape information". These two parameters are not enough to express exactly how the geometric shape changes. If variables such as the surface area and the geometrical center of the chicken breast are also considered and added into the ANN model, the performance of the ANN may improve.

Moreover, this ANN model is based on the assumption that the thickest region is the coldest area without considering the location of the thickest region. All image processing is focused on a ROI. However, if the ROI is located at the edge of the chicken breast, it is possible that it is not the coldest part. In future work, the location information should be considered in the model.

Another point that could be improved is the sampling rate (time between lags). In this study, one reading per ten seconds was tested. The higher the sampling rate, the less the estimation time, but more redundant information is included; the lower the sampling rate, the longer the estimation time, and key

information could be lost. More research is needed to achieve the optimal sample rate and improve the model performance.

Finally, an important point worth mentioning is that the system can be extended by adding a decision and control system as shown in Figure 32. The estimated data can be used to operate a decision system: to condemn, reprocess, or pass the meat. Also, the data can act as a feedback to adjust the cooking procedure by the control unit.

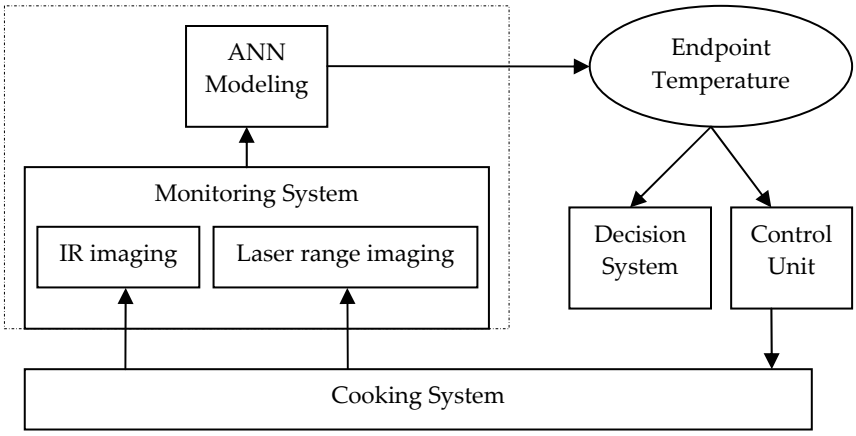

Figure 32. The extended non-invasive endpoint temperature estimation system.

APPENDIX A: Data Acquiring Environment

As shown in Figure A-1, internal temperatures are automatically read into the Excel file using DASwizard software. The first column is time log. The following every three columns are internal temperature readings in chicken breast samples. The temperature readings for four samples are recorded at the same time. The last column is a room temperature reading. The highlight row is the current readings. Figure A-2 shows the IR image grabbing environment. IR images were captured using software Inspector 2.2.

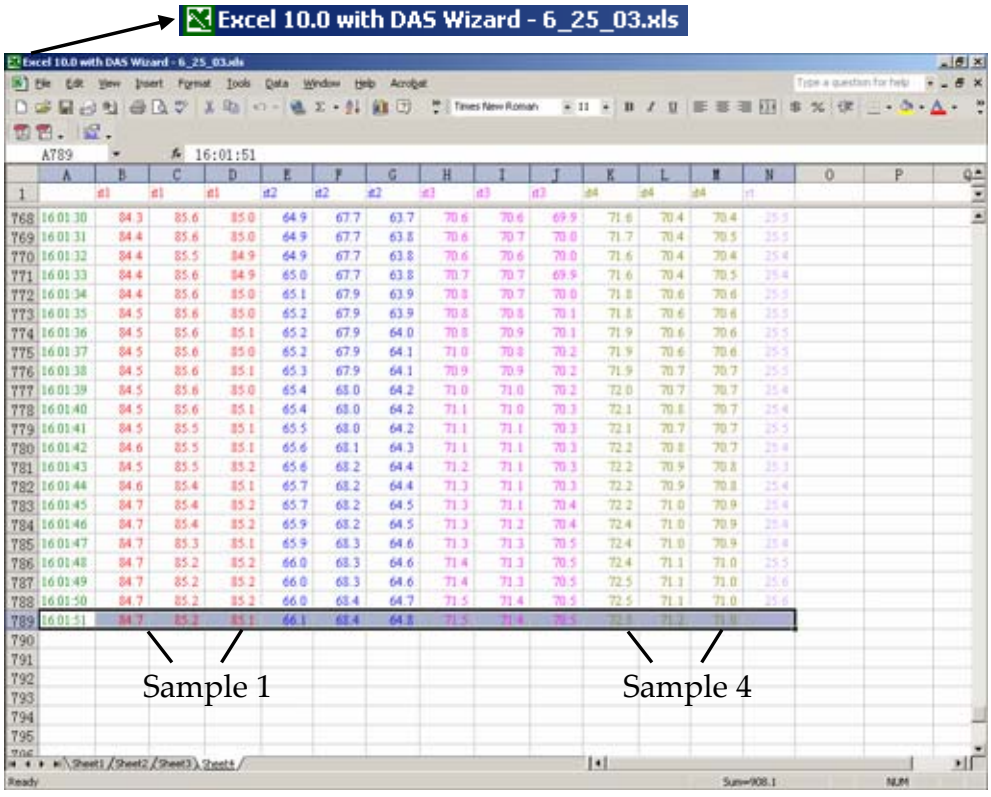

Figure A-1. The internal temperature reading environment.

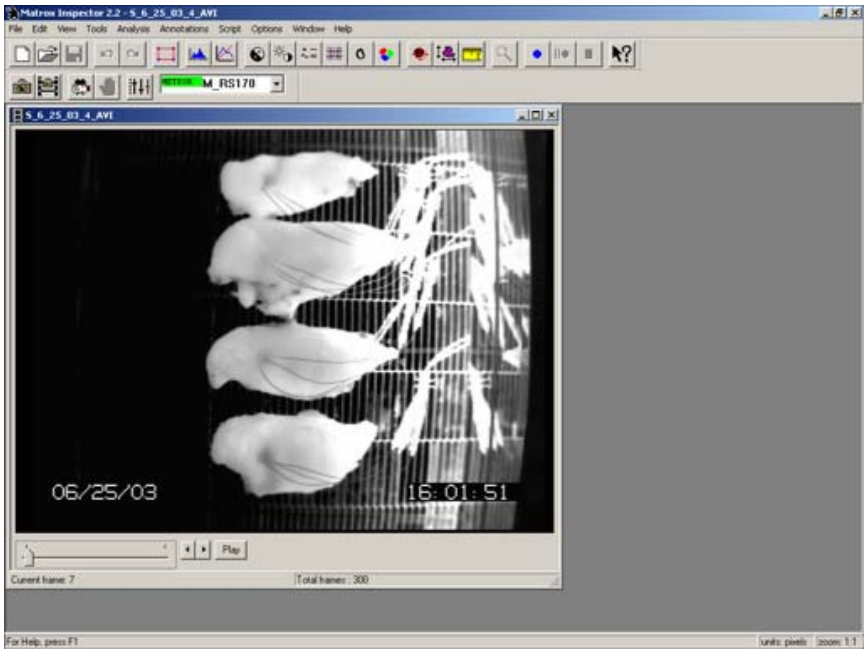

Figure A-2. The IR image grabbing environment.

APPENDIX B: TC Linearity Test Results

Following figures illustrate linearity test results of TC#2 to #12 (Reference temperature: the average reading from the twelve TCs was used as a reference):

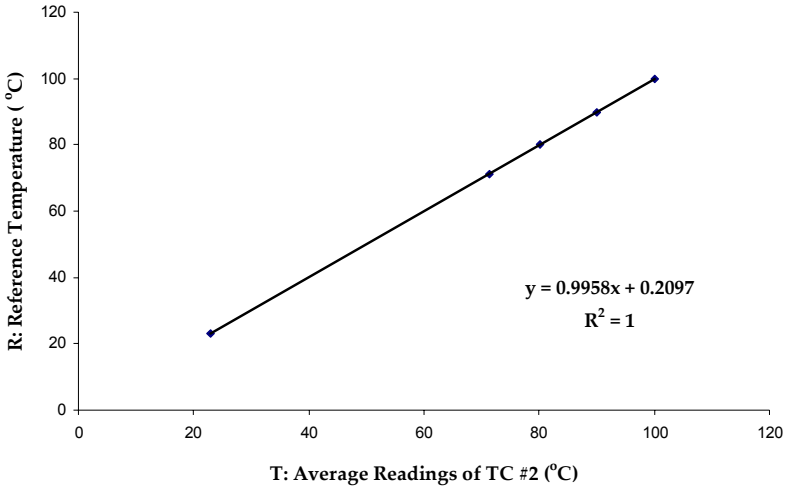

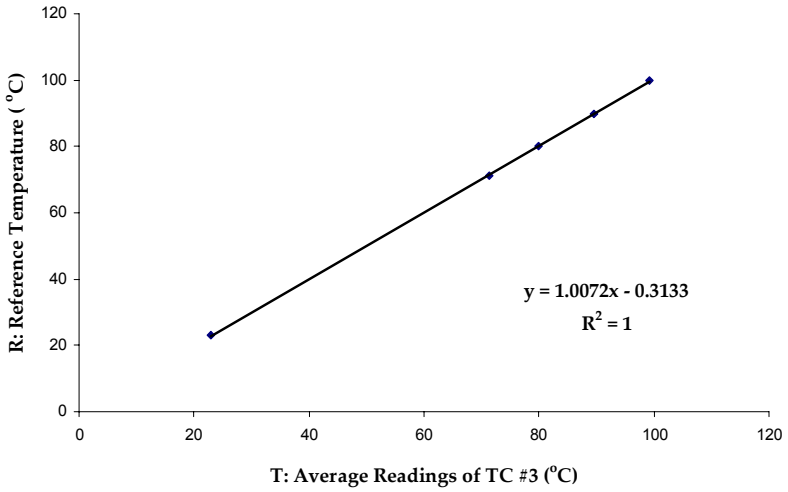

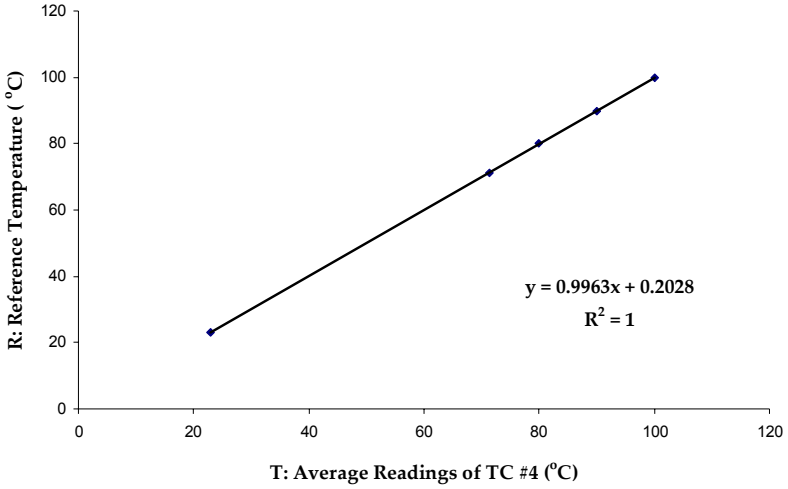
R: Reference Temperature (°C)
T: Average Readings of TC #4 (°C)
y = 0.9963x + 0.2028
R² = 1
0
20
40
60
80
100
120

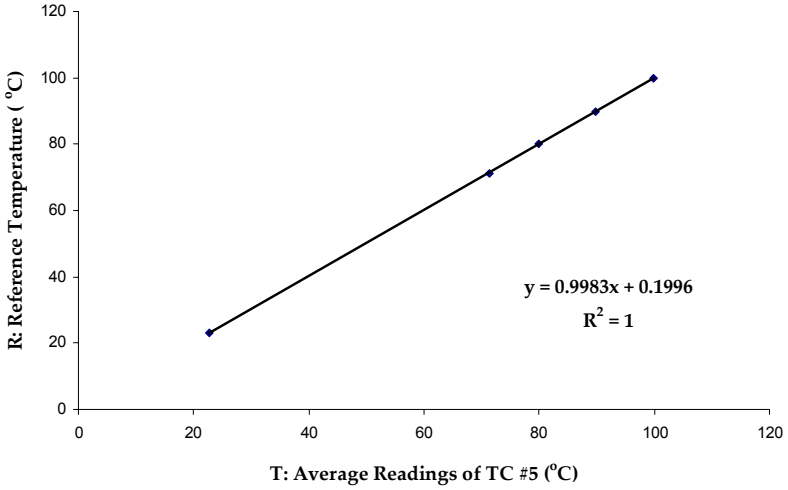
R: Reference Temperature (°C)
T: Average Readings of TC #5 (°C)
y = 0.9983x + 0.1996
R² = 1
0
20
40
60
80
100
120

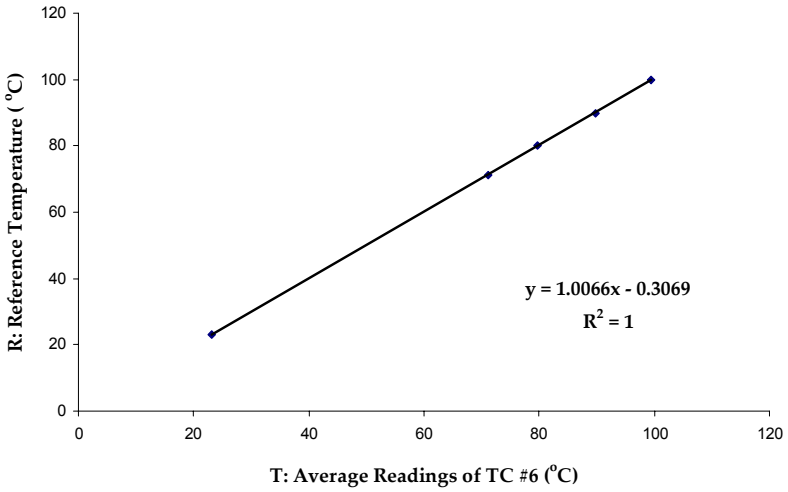
R: Reference Temperature (°C)
T: Average Readings of TC #6 (°C)
y = 1.0066x - 0.3069
R² = 1
0
20
40
60
80
100
120

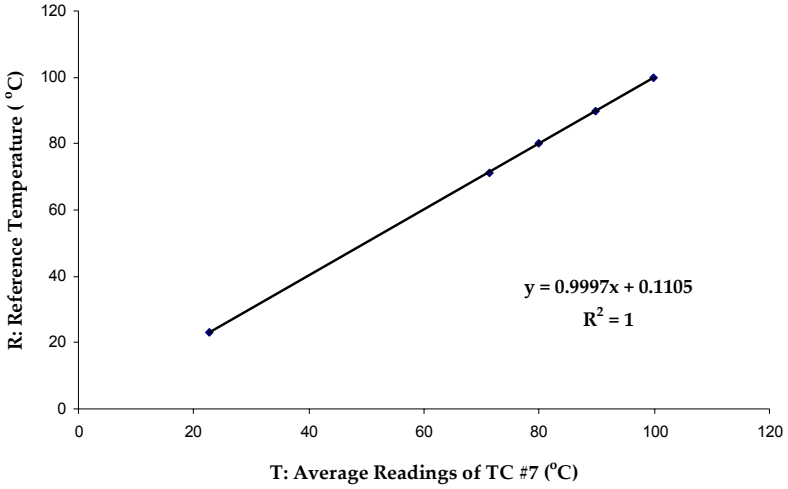
R: Reference Temperature (°C)
T: Average Readings of TC #7 (°C)
y = 0.9997x + 0.1105
R² = 1
0
20
40
60
80
100
120

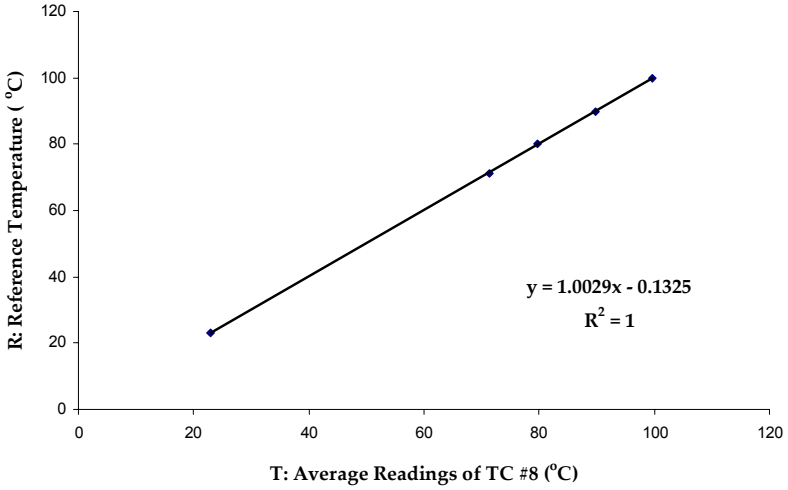
R: Reference Temperature (°C)
T: Average Readings of TC #8 (°C)
y = 1.0029x - 0.1325
R² = 1
0
20
40
60
80
100
120

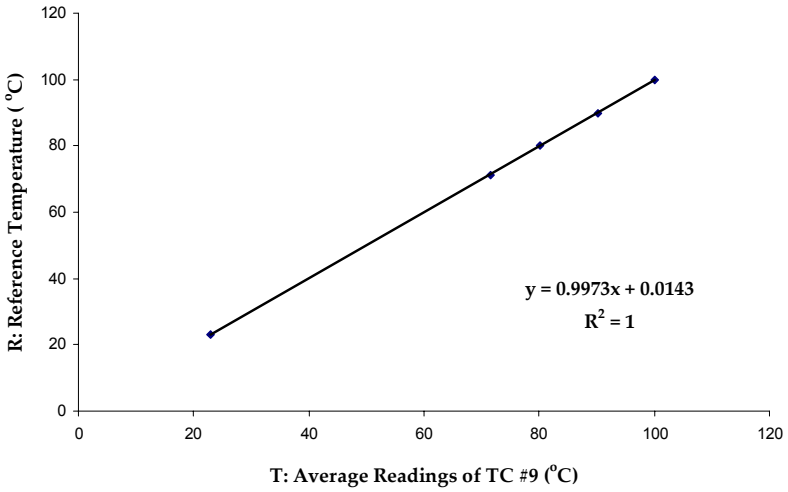
R: Reference Temperature (°C)
T: Average Readings of TC #9 (°C)
y = 0.9973x + 0.0143
R² = 1
0
20
40
60
80
100
120

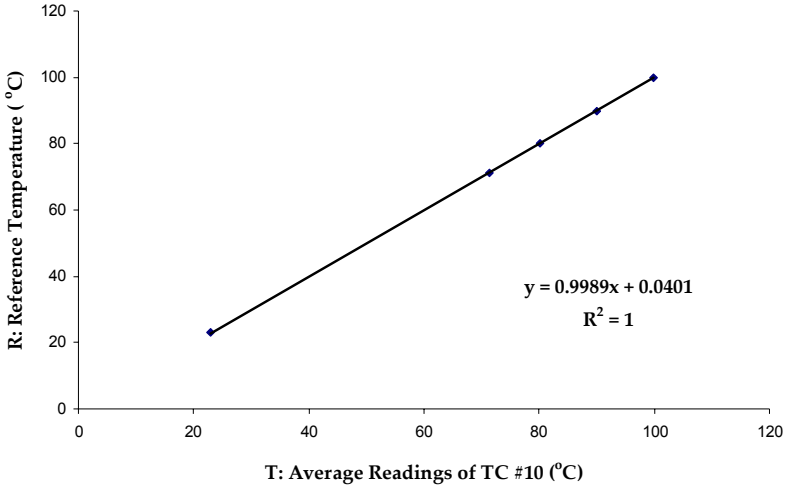
R: Reference Temperature (°C)
T: Average Readings of TC #10 (°C)
y = 0.9989x + 0.0401
R² = 1
0
20
40
60
80
100
120

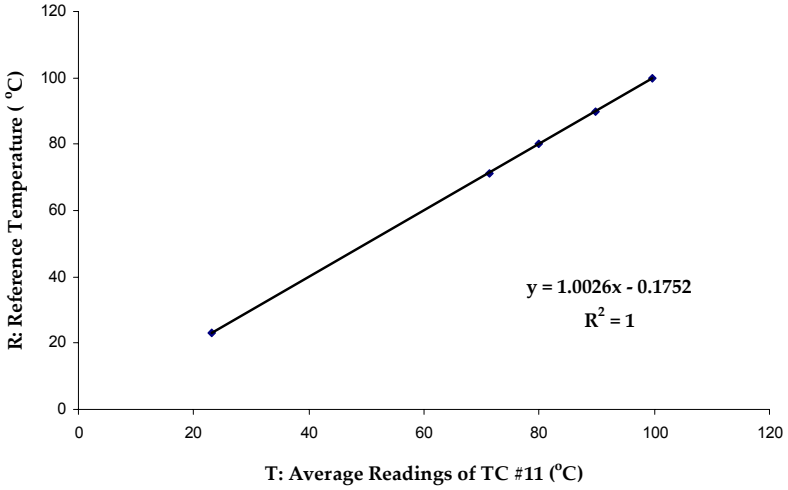
R: Reference Temperature (°C)
T: Average Readings of TC #11 (°C)
y = 1.0026x - 0.1752
R² = 1
0
20
40
60
80
100
120

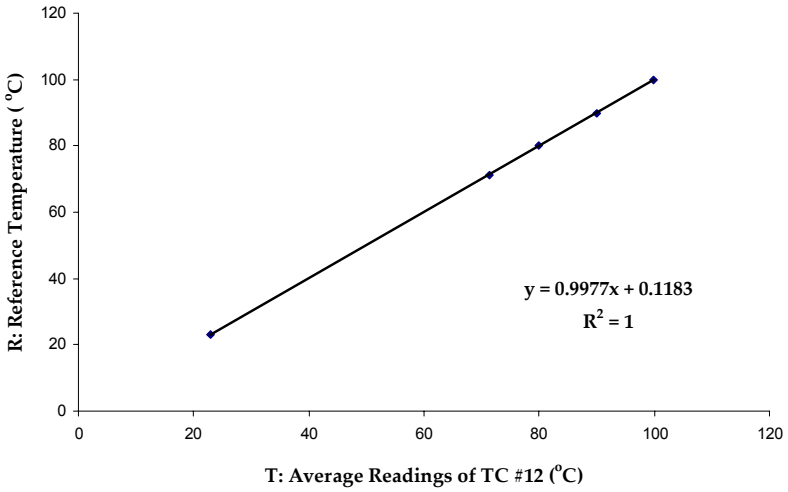
R: Reference Temperature (°C)
T: Average Readings of TC #12 (°C)
y = 0.9977x + 0.1183
R² = 1
0
20
40
60
80
100
120

APPENDIX C: IR and 3D images of Chicken breasts

The following are some IR and 3D images of chicken breasts. Images on the left are 3D images and on the right are the normalized IR images. The red regions are the ROIs.

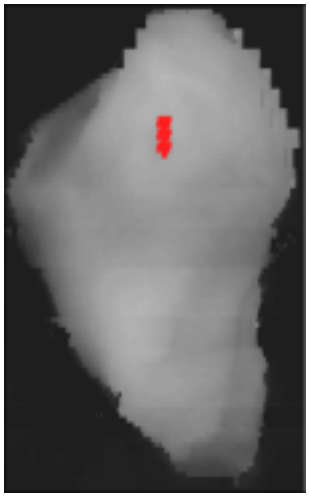

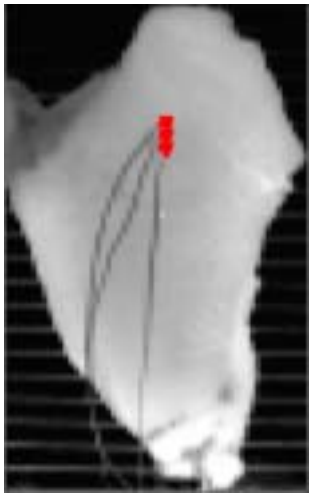

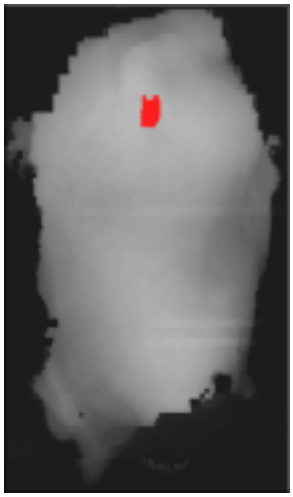

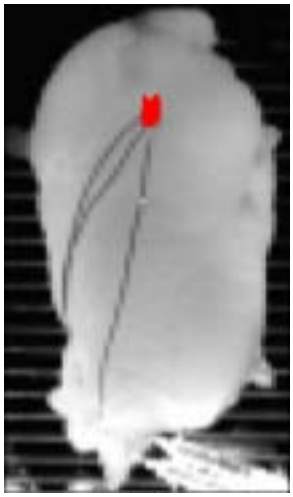

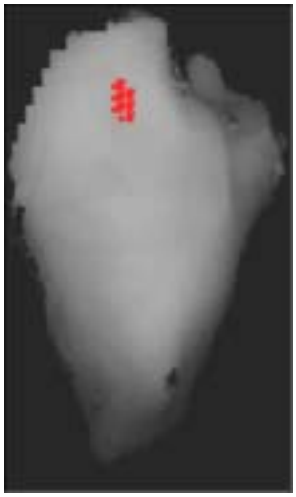

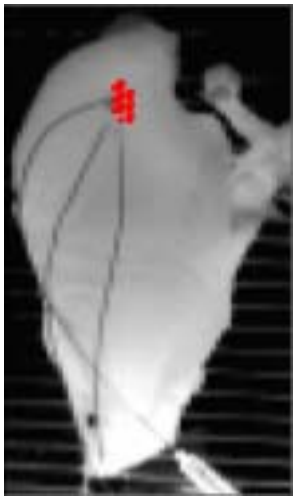

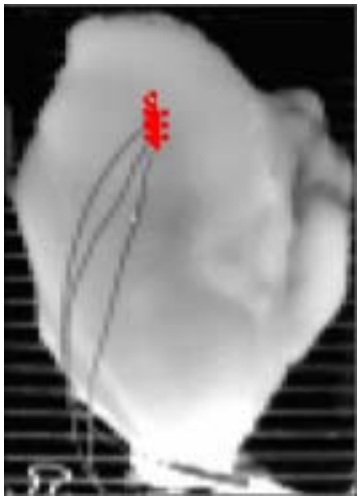

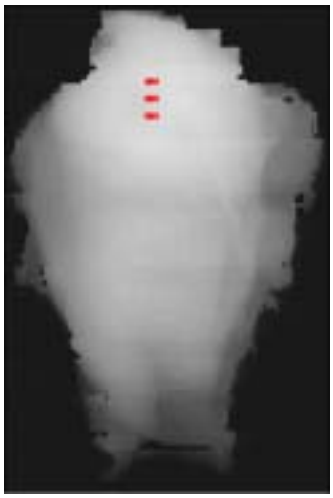

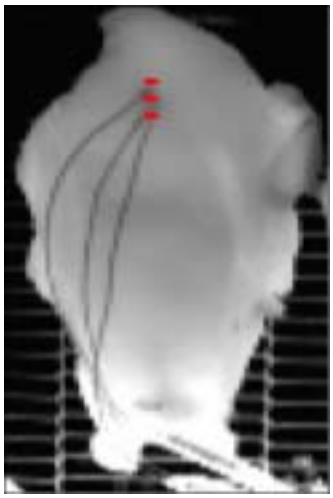

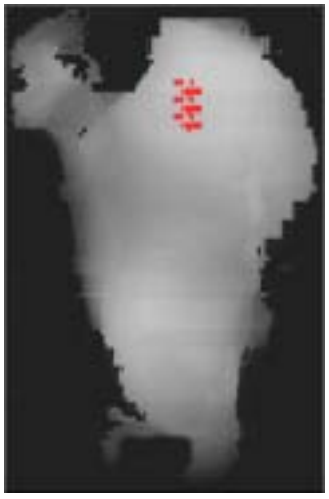

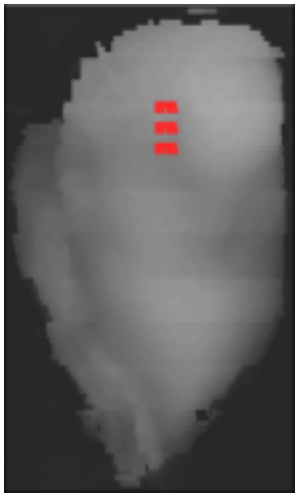

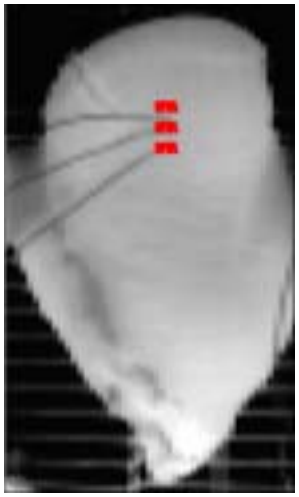

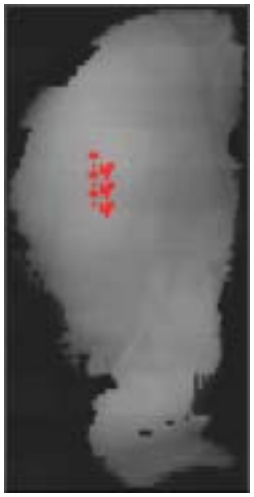

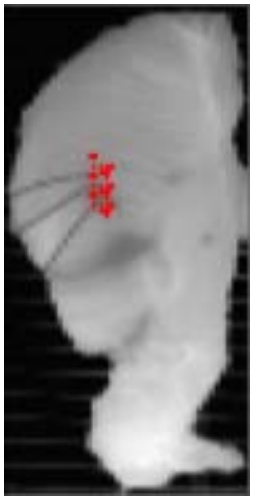

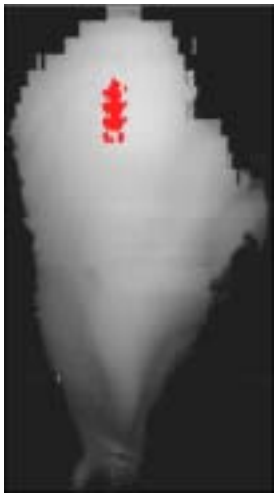

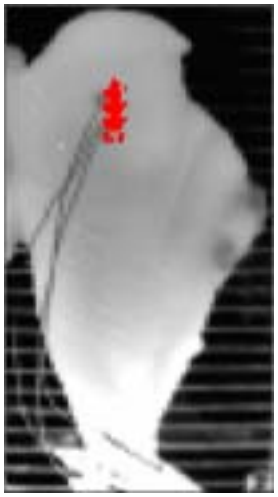

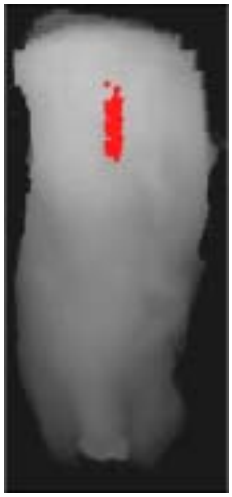

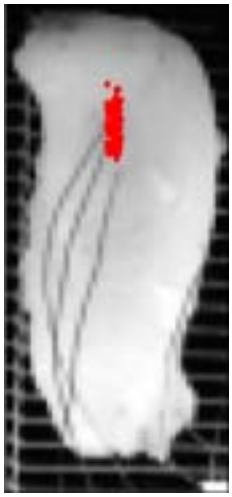

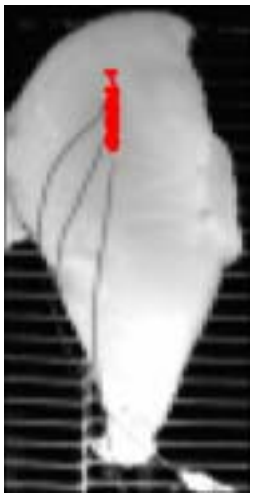

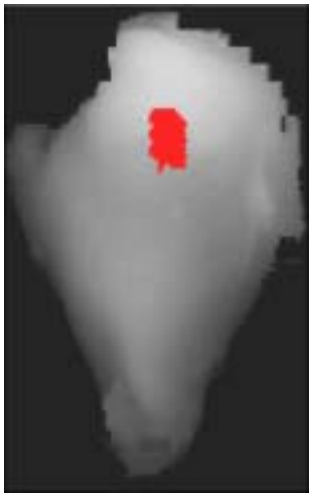

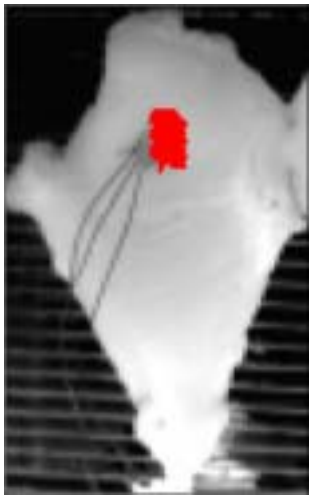

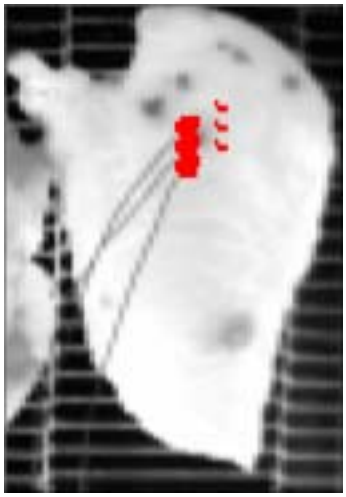

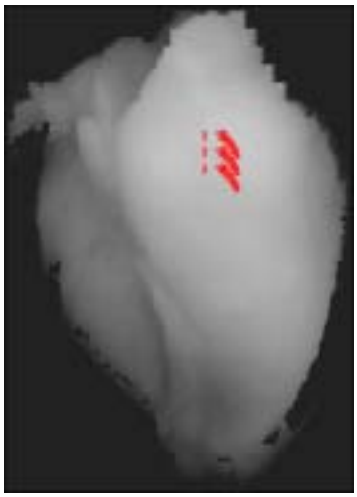

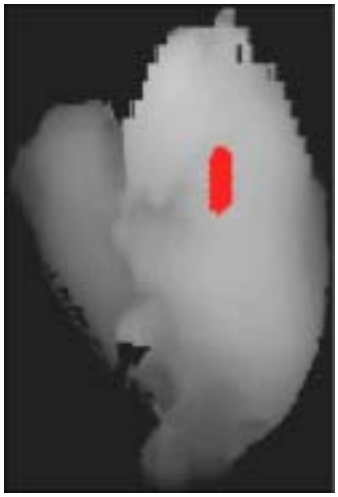

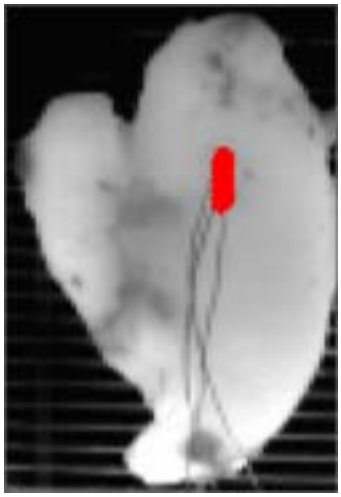

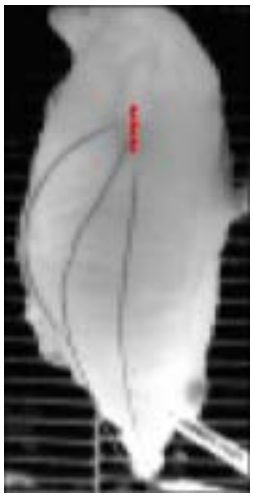

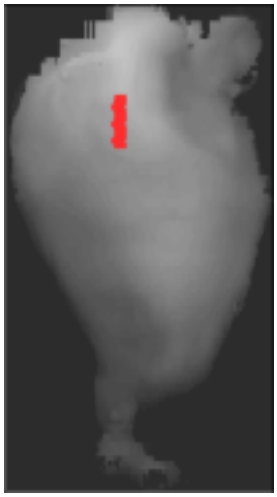

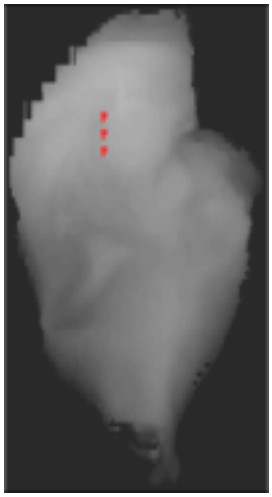

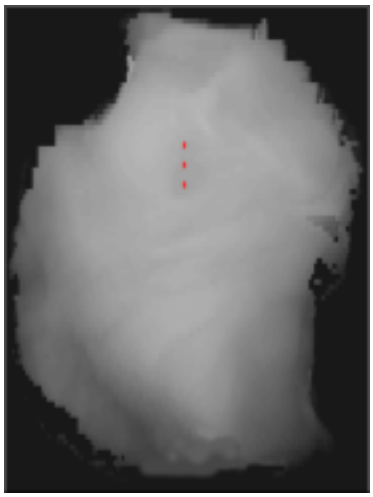
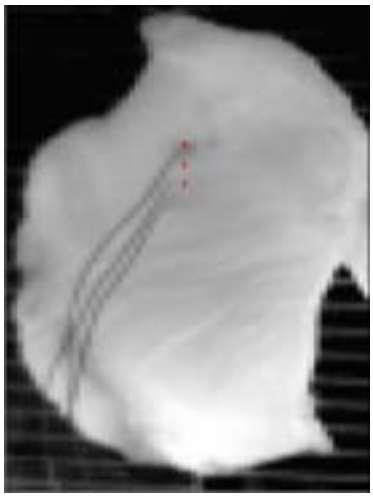
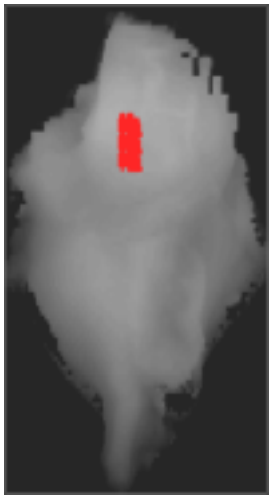

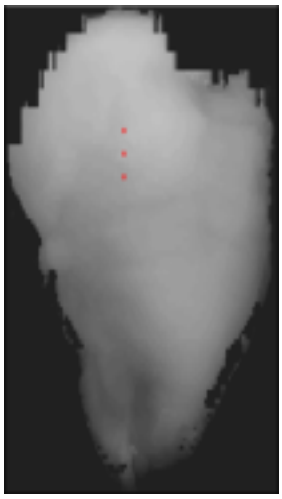
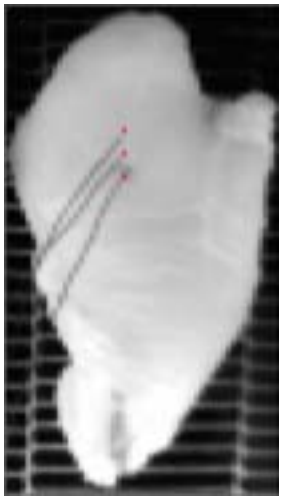

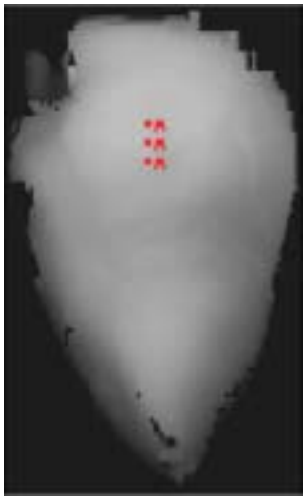

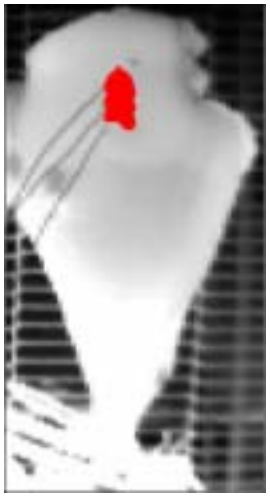

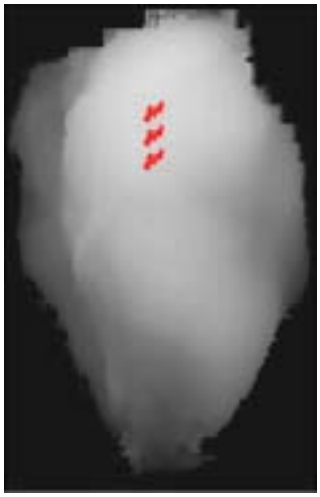

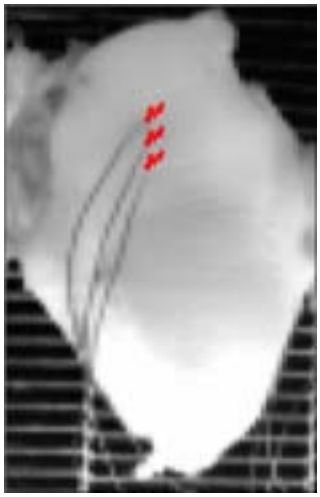

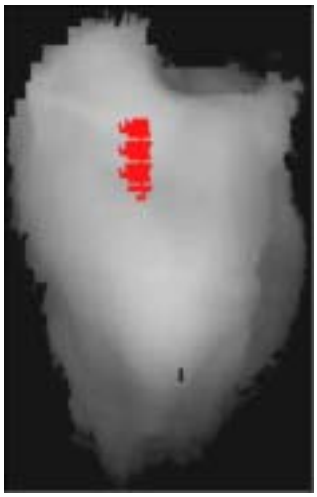

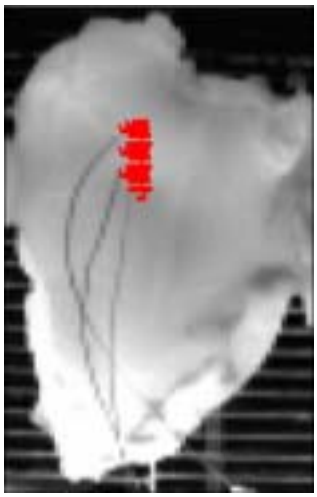

APPENDIX D: Cost of Imaging System

The cost of system equipment:

Components	Price ($)
IR camera	25,000
Oven	7,900
CCD camera	1,400
Laser projector	1,000
PC	1,200
Matrox image board	1,000
Inspector 2.2	1,999
Total	39,499

BIBLIOGRAPHY

Abouzied, M. M., C. H. Wang, J. J. Pestka, and D. M. Smith. 1993. Lactate dehydrogenase as safe endpoint cooking indicator in poultry breast rolls: development of monoclonal antibodies and application to sandwich enzyme-linked immunosorbent assay (ELISA). *Journal of Food Protection* 56(2):120-124.

Acker, D. 1993. An overview of federal food safety research: including research needs for the future. A report by the committee on food, agriculture, and forestry research of the federal coordinating council for science, engineering, and technology. Washington, D.C.

Ang, C. Y. W., F. Liu, and T. Sun. 1994. Development of a dynamic headspace GC method for assessing the influence of heating end-point temperature on volatiles of chicken breast meat. *J. Agric. Food Chem.* 42:2493-2498.

Bean, N. H., J. S. Goulding, M. T. Daniels, and F. J. Angulo. 1997. Surveillance for foodborne disease outbreaks – United States, 1988-1992. *Journal of food protection* 60(10):1265-1286.

Beery, J. T., M. B. Hugdahl, and M. P. Doyle. 1988. Colonization of gastrointestinal tracts of chicks by Campylobacter jejuni. *Applied and Environmental Microbiology* 54:2365-2370.

Buzby, J. C., T. Roberts, C. T. J. Lin, and J. M. MacDonald. 1996. Bacterial foodborne disease: medical costs and productivity losses. Food and Consumer Economics Division, Economic Research Service, U.S. Department of Agriculture. Agricultural Economic Report No. 741. Washington, D.C.

CAST report. 1994. Foodborne pathogens: risks and consequences. Task Force Report No. 122. Washington, D.C.: Council for Agricultural Science and Technology.

Chen, H. and B. P. Marks. 1997. Evaluating previous thermal treatment of chicken patties by visible/near-infrared spectroscopy. *Journal of Food Science* 62(4):753-756, 780.

Cuccurullo, G., P. G. Berardi, R. Carfagna, and V. Pierro. 2002. IR temperature measurements in microwave heating. *Infrared Physics and Technology* 43:145-150.

Danno, A., M. Miyazato, and E. Ishiguro. 1980. Quality evaluation of agricultural products by infrared imaging method III: maturity evaluation of fruits and vegetables. *Mem. Fac. Agr. Kagoshima Univ.* 16:157-164.

D'Aoust, J. Y. 1989. Salmonella. In *Foodborne Bacterial Pathogens,* ed. M. P. Doyle, ch. 9, 327-447. New York, NY: Marcel Dekker Inc.

DePiero, F. W. and M. M. Trivedi. 1996. 3-D computer vision using structured light: design, calibration, and implementation issues. *Advances in computers* 43:243-279.

DeWaal, C. S. 1996. Playing chicken: the human cost of inadequate regulation of the poultry industry. Washington, DC: Center for Science in the Public Interest.

DeWaal, C. S. and K. Barlow. 2002. Outbreak alert! closing the gaps in our federal food-safety net, updated and revised – October, 2001. Washington, DC: Center for Science in the Public Interest.

Doyle, M. P. 1990. Campylobacter jejuni. In *Foodborne Diseases*, ed. D. O. Cliver, ch. 14, 217-223. San Diego, CA: Academic Press.

Doyle, M. P. 1994. The emergence of new agents of foodborne disease in the 1980s. *Food Research International* 27:219-226.

Doyle, M. P. and D. O. Cliver. 1990. Salmonella. In *Foodborne Diseases*, ed. D. O. Cliver, ch. 11, 185-205. San Diego, CA: Academic Press.

Ellekjaer, M. R. and T. Isaksson. 1992. Assessment of maximum cooking temperatures in previously heat treated beef. Part 1: near infrared spectroscopy. *J. Science Food Agri.* 59:335-343.

Fang, H. and D. O. Shah. 1998. The effect of surfactant monolayers on the heat transfer through air/water and oil/water interfaces using IR imaging technique. *Journal of Colloid and Interface Science* 205:531-534.

Foresee, F. D. and M. T. Hagan. 1997. Gauss-Newton approximation to Bayesian learning. In *Proceedings of the 1997 International Joint Conference on Neural Networks*, 1930-1935.

Forsyth, D. A. and J. Ponce. 2003. Computer vision. Upper Saddle River, NJ: Prentice Hall.

FSIS. 2001. Cooking for groups: a volunteer's guide to food safety. [Online]. Available WWW: http://www.fsis.usda.gov/OA/pubs/cfg/cfg7.htm

Goedeken, D. L., C. H. Tong, and R. R. Lentz. 1992. Design and calibration of a continuous temperature measurement system in a microwave cavity by infrared imaging. *Journal of Food Processing and Preservation* 15:331-337.

Hagan, M. T., H. B. Demuth, and M. Beale. 1995. *Neural Network Design*. ch. 1-12. Boston, MA: PWS Publishing Company.

Hagan, M. T. and M. B. Menhaj. 1994. Training feedforward networks with the Marquardt algorithm. *IEEE Transactions on Neural Networks* 5(6):989-993.

Hellebrand, H. J., H. Beuche, M. Linke, B. Herold, and M. Geyer. 2001. Chances and shortcomings of thermal imaging in the evaluation of horticultural products. In *International Conference "Physical Methods in Agriculture - Approach to Precision and Quality"*, 27-30. August 2001.

Hussain, M. A., M. S. Rahman, and C. W. Ng. 2002. Prediction of pores formation (porosity) in foods during drying: generic models by the used of hybrid neural network. *Journal of Food Engineering* 51:239-248.

Ibarra, J. G., Y. Tao, A. J. Cardarelli, and J. Shultz. 2000. Cooked and raw chicken meat: emissivity in the mid-infrared region. *Applied Engineering in Agriculture* 16(2):143-148.

Ibarra, J. G., Y. Tao, J. Walker, and C. Griffis. 1999. Internal temperature of cooked chicken meat through infrared imaging and time series analysis. *Transactions of the ASAE* 42(5):1383-1390.

Ibarra, J. G., Y. Tao, and H. Xin. 2000. Combined IR imaging-neural network method for the estimation of internal temperature in cooked chicken meat. *Optical Engineering* 39(11):3032-3038.

Isaksson T., M. H. R, Ellekjaer, and K. I. Hildrum, 1989. Determination of the previous maximum temperature of heat-treated minced meat by near infrared reflectance spectroscopy. *J. Science Food Agric.* 49:385-387.

Jalkio, J. A., R. C., Kim, and S. K. Case. 1985. Three dimensional inspection using multistripe structured light. *Optical Engineering* 24(6):966-974.

Jing, H. S. 2003. Dynamic 3-D laser range imaging for poultry products. Ph.D. dissertation, Biological Resources Engineering Dept., University of Maryland, College Park.

Labbe, R. 1989. Clostridium perfringens. In *Foodborne Bacterial Pathogens,* ed. M. P. Doyle, ch. 5, 191-234. New York, NY: Marcel Dekker Inc.

Lou, W. and S. Nakai. 2001. Artificial neural network-based predictive model for bacterial growth in a simulated medium of modified-atmosphere-packed cooked meat products. *J. Agric. Food Chem.* 49:1799-1804.

Matrox Inspector 2.2 User's Guide. Quebec, Canada: Matrox Electronics Systems Ltd.

Mittal, G. S. and J. Zhang. 2000a. Use of artificial neural network to predict temperature, moisture, and fat in slab-shaped foods with edible coatings during deep-fat frying. *Journal of Food Science* 65(6):978-983.

Mittal, G. S. and J. Zhang. 2000b. Prediction of freezing time for food products using a neural network. *Food Research International* 33:557-562.

Mittal, G. S. and J. Zhang. 2000c. Prediction of temperature and moisture content of frankfurters during thermal processing using neural network. *Meat Science* 55:13-24.

Mittal, G. S. and J. Zhang. 2001. Artificial neural network for the prediction of temperature, moisture and fat contents in meatballs during deep-fat frying. *International Journal of Food Science and Technology* 36:489-497.

Neural Network Toolbox User's Guide. Natick, MA: The Mathworks Inc.

Nutrition week. 1987. Bacteria-laden meat: who is to blame? 17(15):4-5. Washington, D.C.: Community Nutrition Institute.

Nutrition week. 1987. Congress Scrutinizes Federal Meat Inspection. 17(15):6. Washington, D.C.: Community Nutrition Institute.

Olsen, S. J., L. C. MacKinon, J. S. Goulding, N. H. Bean, and L. Slutsker. 2000. Surveillance for foodborne disease outbreaks – United States, 1993-1997. Division of Bacterial and Mycotic Diseases, National Center for Infectious Diseases. Morbidity and Mortality Weekly Report. CDC Surveill Summ. 49(1):1-62.

Ramesh, M. N., M. A. Kumar, and P. N. S. Rao. 1996. Application of artificial neural networks to investigate the drying of cooked rice. *Journal of Food Process Engg* 19:321-329.

Smith, D. M., L. D., Desrocher, A. M. Booren, C. H. Wang, M. M. Abouzied, J. J. Pestka, and G. J. Veeramuthu. 1996. Cooking temperature of turkey ham affects lactate dehydrogenase, serum albumin and immunoglobulin G as determined by ELISA. *Journal of Food Science* 61(1):209-212.

Sonka, M., V. Hlavac, and R. Boyle. 1999. Image processing, analysis, and machine vision. 2nd edition. Pacific Grove, CA: Brooks/Cole Publishing Company.

Stern, N. J. and S. U. Kazmi. 1989. Campylobacter jejuni. In *Foodbore Bacterial Pathogens,* ed. M. P. Doyle, ch. 3, 71-110. New York, NY: Marcel Dekker Inc.

Tao, Y. 1996. Spherical transform of fruit images for on-line defect extraction of mass objects. *Optical Engineering* 35(2):344-350.

Thodberg, H. H. 1996. A review of Bayesian neural networks with an application to near infrared spectroscopy. *IEEE Transactions on Neural Networks* 7(1):56-72.

Varith, J., G. M. Hyde, A. L. Baritelle, J. K. Fellman, and T. Sattabongkot. 2000. Non-contact bruise detection in apple by thermal imaging. In *Proceeding 8th International Congress for Engineering and Food (ICEF 8),* Puebla, Mexico and *Proceeding for Wm. R. Wiley Research Expo,* Washington State University, Pullman, WA.

Varith, J., G. M. Hyde, J. Tang, and M. J. Pitts. 2001. Validation of bruise detection by thermal imaging using the finite element simulation. In *Uses of thermal properties for nondestructive assessment of apple quality*. Ph.D. Dissertation. Washington State University, Pullman, WA.

Veeramuthu, G. J., A. M. Booren, and D. M. Smith. 1997. Species, muscle type, and formulation influence the residual concentrations of three endpoint temperature indicators in poultry products. *Poultry Science* 76:642-648.

Wang, C. H., A. M. Booren, M. M. Abouzied, J. J. Pestka, and D. M. Smith. 1993. ELISA determination of turkey roll endpoint temperature: Effects of formulation, storage, and processing. *Journal of Food Science* 58:1258-1261, 1264.

Wang, C. H., J. J. Pestka, A. M. Booren, and D. M. Smith. 1994. Lactate dehydrogenase, serum protein, and immunoglobulin G content of uncured turkey thigh rolls as influenced by endpoint cooking temperature. *J. Agric. Food Chem.* 42:1829-1833.

Wen, Z. and Y. Tao. 2000. Dual-camera NIR/MIR imaging for stem-end/calyx identification in apple defect sorting. *Transactions of the ASAE* 43(2):449-452.

Wong, A. C. L. and M. S. Bergdoll. 2002. Staphylococcal food poisoning. In *Foodborne Diseases,* 2nd Edition, ed. D. O. Cliver and H. P. Riemann, ch. 16, 231-248. San Diego, CA: Academic Press.